

Unusual phase behavior of one-component systems with two-scale isotropic interactions

S V Buldyrev¹, G Malescio², C A Angell³, N Giovambattista⁴,
S Prestipino², F Saija⁵, H E Stanley⁶ and L Xu⁷

¹ Department of Physics, Yeshiva University, 500 West 185th Street, New York, NY 10033, USA

² Dipartimento di Fisica, Università degli Studi di Messina, Contrada Papardo, I-98166 Messina, Italy

³ Department of Chemistry and Biochemistry, Arizona State University, Tempe, AZ 85287, USA

⁴ Department of Physics, Brooklyn College of City University of New York, Brooklyn, NY 11210, USA

⁵ CNR-Istituto per i Processi Chimico-Fisici, Contrada Papardo, I-98158 Messina, Italy

⁶ Center for Polymer Studies and Department of Physics, Boston University, Boston, MA 02215, USA

⁷ World Premier International (WPI) Research Center, Advanced Institute for Materials Research, Tohoku University, 2-1-1 Katahira, Aoba-ku, Sendai 980-8577, Japan

Received 14 June 2009

Published 23 November 2009

Online at stacks.iop.org/JPhysCM/21/504106

Abstract

We study the phase behavior of systems of particles interacting through pair potentials with a hard core plus a soft repulsive component. We consider several different forms of soft repulsion, including a square shoulder, a linear ramp and a quasi-exponential tail. The common feature of these potentials is the presence of two repulsive length scales, which may be the origin of unusual phase behaviors such as polyamorphism both in the equilibrium liquid phase and in the glassy state, water-like anomalies in the liquid state and anomalous melting at very high pressures.

(Some figures in this article are in colour only in the electronic version)

1. Introduction

The phase behavior of substances rapidly becomes more variegated as the number of species involved increases and the nature of intermolecular interactions becomes more complicated. However, somewhat surprisingly, even one-component substances characterized by isotropic interactions may show a phase behavior far more complex than that characterizing the more typical simple, i.e. argon-like, fluids. In particular, unusual phase phenomena may be exhibited by spherically symmetric interactions with a softened core. Introducing a finite repulsive component into the interparticle pair potential (which already has a harsh short-range repulsion that accounts for excluded-volume effects) is an idea that dates back to Hemmer and Stell [1, 2]. They considered potentials in which the hard core is softened by adding a square shoulder or

a linear ramp, and focused their investigation on the possible occurrence of multiple critical points and isostructural solid–solid transitions. A few years later, Young and Alder [3] showed that the hard core plus square shoulder potential yields a fluid–solid coexistence line with a maximum melting temperature, similar to that observed in Cs or Ce. Later on, Debenedetti *et al* [4] showed that systems of particles interacting via potentials whose repulsive component presents a downward concavity are capable of losing stability upon supercooling, and of contracting when heated isobarically (giving rise to the so-called density anomaly). Following these pioneering works and during the last decade, potentials with a softened core have been thoroughly investigated for their importance as simplified models for a number of substances such as water, metallic systems and colloidal suspensions and, in general, for their ability to show, within a context that is

relatively easy to study, a wide spectrum of unusual phase phenomena, such as re-entrant melting, liquid–liquid phase transition (LLPT) and water-like anomalies (density, diffusion and structural anomalies) [5–47].

In this paper we review the phase behavior of five softened core interactions: (i) a hard core plus a square shoulder, (ii) a hard core plus a linear ramp, (iii) a hard core plus a combination of a square shoulder and a square well (SSSW), (iv) a hard core plus a combination of repulsive and attractive ramps (the Jagla potential) and (v) the exp-6 potential. For the shoulder and SSSW potentials the forces are delta functions of the distance, for the ramp potentials, the strength of the repulsive force is constant over an interval of interparticle distances r , while for the exp-6 potential, for a range of r values, the repulsive force decreases as the distance gets smaller. This peculiar repulsion enables us to identify two length scales: a larger one, associated with the external finite repulsion (effective at lower pressures and temperatures), and a smaller one, related to the particle hard core (dominant at higher pressures and temperatures). It follows that in those thermodynamic regimes where the two length scales are both partially effective and thus are competing with each other, a system of particles interacting through such potentials behaves, in many respects, as though it were a mixture of two species of different sizes. This may explain the origin of several interesting phase behaviors.

This paper is organized as follows. In section 2 we review the properties of the square shoulder, SSSW, ramp and Jagla potentials in terms of their ability to reproduce the water-like anomalies, glass transition and the LLPT. A special emphasis is given to the effects of the attractive part of the potential. In section 3 we review the occurrence of re-entrant melting and related anomalous behavior for the exp-6 interaction model.

2. Liquid anomalies, polyamorphism and LLPT

2.1. Soft core potentials

Soft core potentials have a long history of being used to model isostructural critical points in crystals [1–3], polymorphism of crystal phases [13, 15, 40, 41], LLPTs [4, 10, 15, 16, 20, 23, 25, 42], polyamorphism in glasses [17, 28, 30, 33, 37] and anomalous thermal expansion of liquids at low temperatures [4, 7–12, 15, 28, 29, 31, 32, 35, 39, 43]. All these phenomena can be associated with the existence of two competing local structures: an expanded structure characterized by large open spaces between particles, and a collapsed structure in which particles are spaced more closely. The expanded structure is the result of quantum mechanical interactions between particles, interactions that differ depending upon the material. For example, in water the expanded structure is caused by four-coordinated hydrogen bonds that build a first coordination sphere of only four molecules [23, 36, 48–56], while in simple liquids, such as argon, the first coordination sphere consists of approximately twelve particles arranged in a closely packed configuration. Accordingly, water has much more empty space between molecules than argon and its density can be significantly increased by increasing the pressure which distorts the

hydrogen bond structure and increases the number of particles in the first coordination sphere [8]. This distortion is associated with an increase in entropy and hence with a density anomaly due to the Maxwell relation

$$\alpha_P = \frac{1}{V} \left(\frac{\partial V}{\partial T} \right)_P = -\frac{1}{V} \left(\frac{\partial S}{\partial P} \right)_T < 0, \quad (1)$$

where α_P is the thermal expansion coefficient. The increase in entropy due to an increase in pressure can also, under certain conditions, be associated with an anomalous increase of diffusivity. This can be seen from the Adam–Gibbs relation [12, 57]

$$D \sim \exp(-A/TS_{\text{conf}}), \quad (2)$$

where A is a positive activation energy and S_{conf} is the configurational entropy—if we assume that the behavior of configurational entropy with pressure is similar to the behavior of total entropy. The local order parameters [58, 59] are related to entropy and to excess entropy, S_{ex} . Therefore various order parameters, density and diffusivity usually form a ‘cascade of anomalies’ on the P – T plane, such that the region of anomalous behavior of one parameter encloses the region of anomalous behavior of another. The location of these lines can be approximately determined by the equation

$$\left(\frac{\partial S_{\text{ex}}}{\partial \ln \rho} \right)_T = ck_B, \quad (3)$$

in which different values of c correspond to different parameters [60, 61]. Soft core potentials often reproduce this cascade of anomalies [29, 31, 60].

The collapse of the open structure under pressure leads at low temperatures to two distinct glassy states (polyamorphism): low density amorphous solid (LDA) and high density amorphous solid (HDA), which transform into one another by pressurizing and depressurizing. This transformation between two glassy states is associated with hysteresis [17, 37, 62].

The interplay between two local structures at intermediate temperatures above the glass transition may lead under certain conditions to their spatial segregation and hence to an LLPT, the existence of which is hypothesized in water based on computer simulations [63] and the extrapolation of the heat capacity [64]. A direct observation of the LLPT has been made in yttrium aluminum garnet ($\text{Y}_3\text{Al}_5\text{O}_{12}$) [65, 66]. The LLPT associated with the transformation from molecular to polymeric liquid has been theoretically predicted [67] and experimentally observed in liquid phosphorus [68, 69]. Polyamorphism recently has been observed in cerium-based metallic glasses ($\text{Ce}_{55}\text{Al}_{45}$) [70] in which the transition is caused by pressure-induced f-electron delocalization. There is a growing body of evidence, both experimental and computational, that LLPTs and polyamorphic glasses may exist at high temperatures and pressures in group IV elements: silicon [71–73] and germanium [74–76], certain molecular compounds such as silica (SiO_2) [77–79] and ionic salts such as BeF_2 [80]. All these substances have tetrahedral local symmetry. There is indirect experimental evidence for an

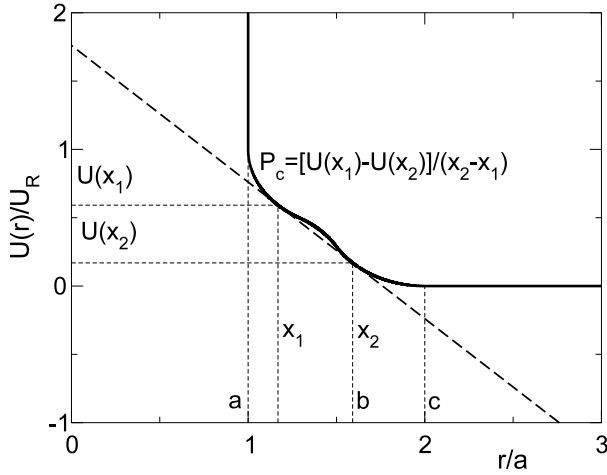


Figure 1. A typical soft core potential $U(r)$ (solid line) with two repulsive scales: hard core a and soft core b . If the maximal range of potential $c \leq 2a$, the one-dimensional model has an exact solution which displays a first-order phase transition at $P = P_c$, $T \rightarrow 0$ where the average interparticle distance (one-dimensional volume) discontinuously changes from $x = x_1$ for $P > P_c$ to $x = x_2$ for $P < P_c$, where P_c , x_1 and x_2 can be found by the Maxwell construction (dashed inclined line). The one-dimensional model has a region of density anomaly near $T = 0$, $P = P_c$.

LLPT in sulfur [81–83], selenium [84] and some molecular liquids [66, 85, 86]. *Ab initio* computer simulations suggest that LLPTs may exist in hydrogen [87–89] and nitrogen [90] at high pressures and temperatures. Since the direct experimental observation of LLPT is often difficult, its existence can be hypothesized based on observation of other experimental features of the system which are usually associated with LLPT, e.g. the melting line maximum, the presence of rich crystal polymorphism [8], the presence of density or diffusivity anomalies, or an increase in heat capacity or compressibility when cooled.

All of these examples show that liquid anomalies and polyamorphism, although caused in different materials by different chemistries, have similar physics: namely all these substances have large open spaces between particles that collapse under pressure. Thus we need a simple, universal model that can determine whether these features and phenomena are related or exist independently. The simplest model that satisfies these conditions is a spherically symmetric potential (figure 1) that has two distinct length scales: a soft core b , which creates a low density structure at low pressure, and a smaller hard core a , which creates a high density structure. In principle, the hard core diameter a can be zero (like in a Gaussian potential studied in [9]). These simple models typically possess a rich crystalline polymorphism and, under certain conditions, exhibit liquid anomalies and polyamorphism. Here we will review recent studies showing how the various properties of a potential determine a system's propensity to have liquid anomalies and polyamorphism in glassy or liquid phases and whether these phenomena can exist independently of each other.

2.2. One-dimensional solution

Although soft core potentials are simple, the exact analytical solution for them exists only in a one-dimensional case provided the maximal range of the potential, c ($U(r) = 0$ for any $r > c$), obeys the condition $c < 2a$ (figure 1), which restricts the interactions to nearest neighbors. Under these conditions, the partition function can be factorized, and there exists a Takahashi solution for the Gibbs potential [7, 10, 11, 28]:

$$G(P, T) = -k_B T N \ln \int_0^\infty \exp\left[-\frac{U(x) + Px}{k_B T}\right] dx. \quad (4)$$

Therefore, the equation of state is

$$v = \langle x \rangle = \int_0^\infty x p(x) dx, \quad (5)$$

where v is the volume per particle, which in one dimension is equal to the average interparticle distance, and $p(x)$ is the probability that two neighbors will be separated by a distance x , which is given by the normalized Boltzmann factor

$$p(x) = \exp\left[-\frac{U(x) + Px}{k_B T}\right] / \int_0^\infty \exp\left[-\frac{U(x) + Px}{k_B T}\right] dx. \quad (6)$$

It is straightforward to show that, for $P = -U'(x)|_{x=v}$, such that $U''(x) > 0$:

$$\lim_{T \rightarrow 0} \left(\frac{\partial v}{\partial T} \right)_P = -\frac{k_B U'''(x)}{2[U''(x)]^2}. \quad (7)$$

Thus the sufficient condition for the density anomaly is $U'(x) < 0$, $U''(x) > 0$, $U'''(x) > 0$.

Since at $T = 0$ the Gibbs potential coincides with enthalpy $H(v) = U(v) + Pv$, a sufficient condition for a phase transition at $T = 0$, $P = P_c$ is the existence of two points $x_1 < x_2$ that satisfy a Maxwell construction on the potential energy graph (figure 1), such that $U'(x_1) = U'(x_2) = -P_c$, $U(x_2) - U(x_1) = -P_c(x_2 - x_1)$ and, for any x between x_1 and x_2 , $U(x) \geq U(x_1) - P_c(x - x_1)$. For a discontinuous potential, x_1 and x_2 are the values of the discontinuity of the potential (figure 2(a)) or its first derivative (figure 3(a)). Obviously, a potential with a linear ramp between x_1 and x_2 or a potential with a square shoulder satisfies these conditions. Note that $x_1 = \lim_{T \rightarrow 0} v|_{P > P_c}$ gives the volume of the high density phase, while $x_2 = \lim_{T \rightarrow 0} v|_{P < P_c}$ is the volume of the low density phase. If there are several ramps or several shoulders in the potential, each of them produces an additional phase transition at $T = 0$. It can be shown that

$$v_c \equiv \lim_{T \rightarrow 0} v(P_c) = p_1 x_1 + p_2 x_2, \quad (8)$$

where $p_1 > 0$ and $p_2 > 0$ ($p_1 + p_2 = 1$) gives the probabilities of x_1 and x_2 , which can be computed from $p(x)$ using the Laplace method for $T \rightarrow 0$. Thus $x_1 < v_c < x_2$ and hence, for P slightly less than P_c and T slightly above zero, v must increase upon cooling, going from $v = v_c + \epsilon$ at $T = \delta T > 0$ to $v = x_2$ at $T = 0$. Thus in one dimension the region of the density anomaly must necessarily exist if the phase transition exists at $T = 0$. But the density anomaly can exist in the absence of the phase transition.

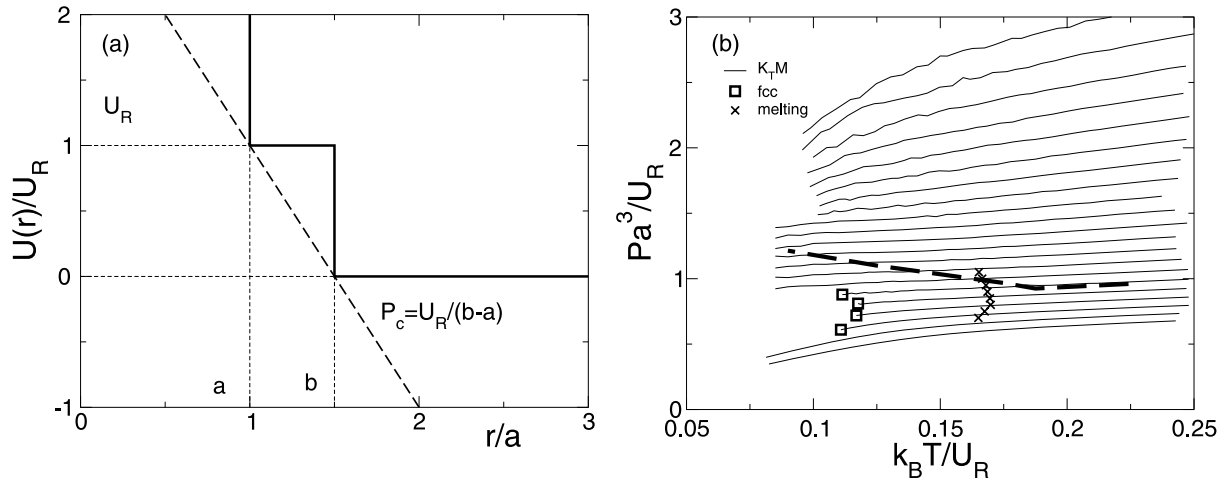


Figure 2. (a) A discontinuous square shoulder potential $U(r)$ (solid line) with two repulsive scales: hard core a and soft core b . If the maximal range of potential $b \leq 2a$, the one-dimensional model has an exact solution which displays a first-order phase transition at $P = P_c = U_R/(b - a)$, $T \rightarrow 0$, where the average interparticle distance (one-dimensional volume) discontinuously changes from $x = a$ for $P > P_c$ to $x = b$ for $P < P_c$. P_c can be found by the Maxwell construction (dashed inclined line). The one-dimensional model has a region of density anomaly near $T = 0$, $P = P_c$. (b) P - T phase diagram of the shoulder potential for $b = 1.5a$ in three dimensions. Thin lines are isochores for 21 different densities between $\rho = 0.593a$ and 0.292 , corresponding to the system of $N = 2000$ particles in the cubic box with the edge $L = 15.0a, L = 15.2a \dots L = 19.0a$. The isochores are interrupted at low temperatures either by spontaneous crystallization into a face-centered cubic (fcc) crystal (\square) or due to insufficient equilibration time as the system approaches glass transition. The fcc crystal melts at much higher temperatures, displaying the melting temperature maximum indicated by the ‘ \times ’ symbols. The three-dimensional model lacks liquid–liquid phase transition, and density and diffusivity anomaly. It displays the anomalous increase of isothermal compressibility upon cooling for the pressures above the thick dashed line which indicates compressibility minima and maxima as a function of temperature at constant pressure.

2.3. Simulations in three and two dimensions

Exact solutions do not exist in two and three dimensions, and Monte Carlo (MC) or molecular dynamics (MD) simulations are the only reliable methods of obtaining the equation of state. But, at low temperatures, systems in two and three dimensions crystallize or become non-ergodic due to the glass transition, and thus we cannot obtain an equilibrium liquid equation of state. Therefore, the class of potentials for which the LLPT can be directly observed between two stable or metastable liquid states is actually rather narrow. In some cases one can argue that the position of the liquid–liquid critical point (LLCP) can be obtained by extrapolating the equation of state from the region that allows equilibrium measurements [12, 28], but here we will report only the features that can be clearly identified through MC or MD simulations. Two-dimensional simulations have their own specifics related to the quasi-continuous nature of liquid–solid transitions in two dimensions [43]. Two-dimensional studies are addressed in [10, 12, 13, 16, 17, 23, 40, 41, 43].

Two types of soft core potential have been investigated: (i) potentials with an attractive part characterized by the existence of a range of interparticle distances r in which $U(r) < 0$ [10, 16, 20, 37] (figures 4(a) and 5(a)) and (ii) purely repulsive potentials for which $U(r) \geq 0$ for any r [13, 15, 28, 29, 31, 39–41, 47] (figures 2(a) and 3(a)).

2.4. Purely repulsive soft core potentials

Among the purely repulsive soft core potentials that have been studied are (i) the Gaussian potential [9], which has

both density and diffusivity anomalies as well as a re-entering melting line, (ii) the square shoulder potential [3] (figure 2) and (iii) the ramp potential [13, 15] (figure 3(b)) and probably polyamorphism [17, 28]. There is a hysteretic transition between high density glass and low density glass at low temperatures [17]. These glasses are characterized by distinct static structure factors that determine the behavior of the non-ergodicity parameters of the mode-coupling theory [28]. Similar continuous potentials with long repulsive tails have been studied by Camp [40, 41] in two dimensions, who observe rich crystal polymorphism, density and diffusion anomaly, as well as rich polyamorphism with gradual transformation between amorphous structure characterized by different degrees of clustering, but no evidence of the LLPT, or sharp first-order-like transformations between different types of glasses.

The ramp potential exhibits density, diffusion and structural anomalies in the wide range of $\lambda = a/b$ [29, 31], rich crystal polymorphism [13, 15] (figure 3(b)) and probably polyamorphism [17, 28]. There is a hysteretic transition between high density glass and low density glass at low temperatures [17]. These glasses are characterized by distinct static structure factors that determine the behavior of the non-ergodicity parameters of the mode-coupling theory [28]. Similar continuous potentials with long repulsive tails have been studied by Camp [40, 41] in two dimensions, who observe rich crystal polymorphism, density and diffusion anomaly, as well as rich polyamorphism with gradual transformation between amorphous structure characterized by different degrees of clustering, but no evidence of the LLPT, or sharp first-order-like transformations between different types of glasses.

The parameters of the ramp can be adjusted in such a way that its phase diagram quantitatively resembles the phase diagrams of TIP5P water [36]. The crucial point in the identification is to assume that the radius of the first

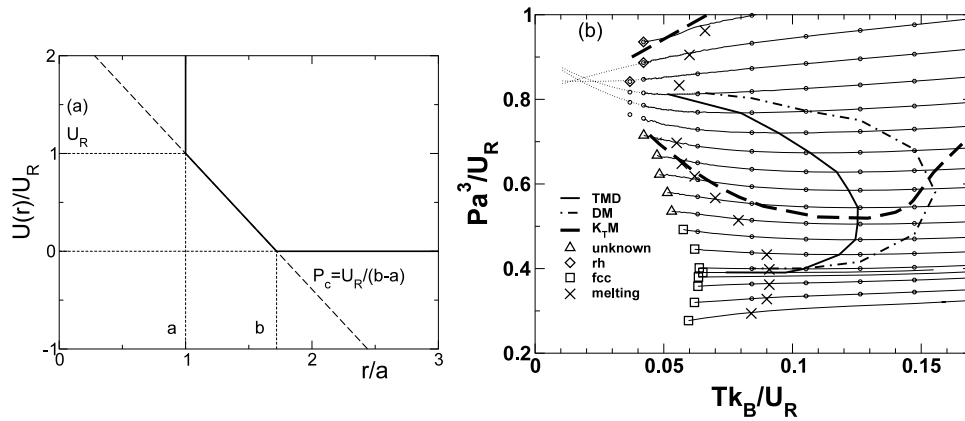


Figure 3. (a) A ramp potential $U(r)$ (solid line) with two repulsive scales: hard core a and soft core b , introduced by Jagla [13, 15]. If the maximal range of potential $b \leq 2a$, the one-dimensional model has an exact solution which displays a first-order phase transition at $P = P_c = U_R/(b-a)$, $T \rightarrow 0$, where the average interparticle distance discontinuously changes from $x = a$ for $P > P_c$ to $x = b$ for $P < P_c$. P_c can be found by the Maxwell construction (dashed inclined line). The one-dimensional model has a region of density anomaly near $T = 0$, $P = P_c$. (b) P - T phase diagram of the ramp potential for $b = 1.72a$ in three dimensions [28]. Thin lines are isochores for 17 different densities between $\rho = 0.377a^{-3}$ and $0.223a^{-3}$, corresponding to the system of $N = 1728$ particles in the cubic box with the edge $L = 16.6a$, $L = 16.8a \dots L = 19.8a$. Two additional isochores correspond to densities $\rho = 0.242a^{-3}$ and $0.240a^{-3}$ for which the density minimum is observed. The isochores are interrupted at low temperatures either by spontaneous crystallization or due to insufficient equilibration time as the system approaches the glass transition. The system crystallizes into several polymorphs including fcc, hexagonal close packed (hcp) and rhombohedral (rh). Some crystal structures are too disordered to be unambiguously identified from computer simulations, but most probably they are mixtures of fcc and hcp with many stacking faults. The equilibrium melting line (\times) of the fcc crystal displays a clear maximum. The model displays a density anomaly bounded by the temperature of maximum/minimum density (TMD) line (bold). It is crossed by the compressibility maximum/minimum line ($K_T M$) line (dashed line). The region of density anomaly is enclosed by the region of diffusivity anomaly, bounded by the diffusivity minimum/maximum (DM) line (dash-dotted line). The three-dimensional model lacks liquid-liquid phase transition in the region of the PT phase diagram accessible in simulations: however, some isochores cross upon extrapolation (dotted lines) at low temperatures, suggesting the possible existence of the fluid-fluid critical point. We can observe also a high density branch of compressibility maxima, which may indicate the presence of the Widom line emanating from the critical point. This line must join the compressibility minima line at high temperatures. The heat capacity increases upon cooling in the entire displayed region of the phase diagram.

coordination shell in water coincides with the hard core diameter of the potential, while the radius of the second coordination shell coincides with the soft core diameter of the potential. The first coordination shell in water effectively corresponds to two water molecules: a central molecule and four quarters of its nearest neighbors. This structural unit, expressed by the chemical formula $O(\text{HO}_{1/4})_4$, provides the building blocks for a hexagonal ice crystal, which is a hexagonal close packed (hcp) lattice assembled from such units. Of note is that ramp models crystallize at low pressures either into an hcp or a face-centered cubic (fcc) crystal whose density is lower than the density of liquid, in complete agreement with the behavior of water in which the density of ice is lower than the density of liquid (figure 3(b)). Accordingly, two water molecules correspond to one ramp particle and the number density of water is two times larger than the corresponding number density of the ramp model. The pairs of particles that are at the hard core distance in the ramp model correspond to the water molecules with five nearest neighbors, i.e. when a molecule from the second coordination shell enters the first coordination shell [8, 55, 56]. This fifth neighbor leads to the hydrogen bond bifurcation associated with an increase of potential energy equivalent to the energy of the repulsive ramp. The diffusivity of water is related to the hydrogen bond exchange between diffusing molecules. Therefore it is proportional to the number of

bifurcated hydrogen bonds, and hence to the number of five-coordinated molecules that increase with pressure. Therefore the diffusivity of water increases with pressure. The same is true of the diffusivity of the ramp model within a certain range of densities. Indeed, at the density corresponding to the density of closely packed soft cores, the diffusivity will take place only if the particles can climb up the repulsive ramp. Therefore the diffusivity is proportional to the number of particles with a nearest neighbor inside the repulsive ramp. Obviously the number of such particles increases with pressure as figure 6 suggests for a similar model.

In general, a particle in a soft core model may be regarded as a coarse-grained representation of the structural chemistry of a real liquid with anomalous behavior. It is not surprising that such macroscopic collective phenomena as phase transitions arise on scales exceeding an atomic diameter. At such scales the specific chemical nature of interatomic interactions is washed away, and the behavior of the system can be adequately quantified by studying the interaction of larger structural units using an appropriately parameterized binary spherically symmetric potential. Obviously a soft core potential cannot predict the electronic properties of a system because that level of detail is deliberately excluded from the model. It is still remarkable that the soft core potential can mimic many properties of real substances if the correct parameters are used.

The fact that the potential parameters must be selected with care is illustrated by the square shoulder potential

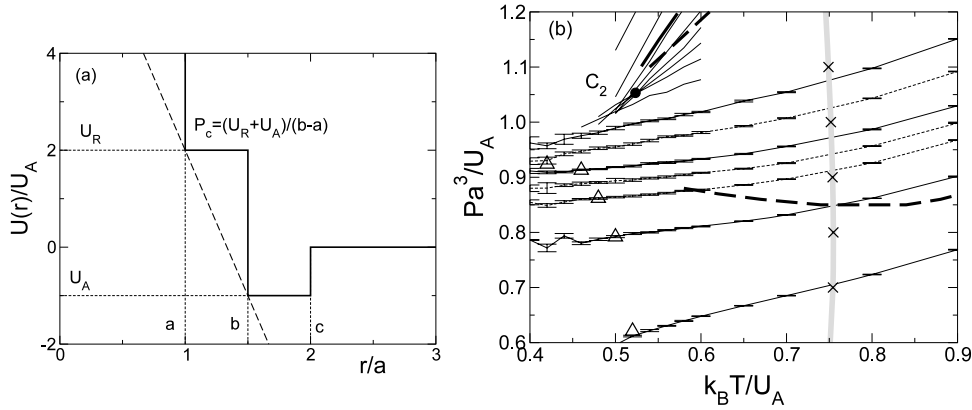


Figure 4. A square shoulder square well potential (SSSW) [26]. (a) $U(r)$ (solid line) with two repulsive scales: hard core a and soft core b and a square well of diameter c . The height of the shoulder is U_R and the depth of the well is U_A . If the maximal range of potential $c \leq 2a$, the one-dimensional model has an exact solution which displays a first-order phase transition at $P = P_c = (U_R + U_A)/(b - a)$, $T \rightarrow 0$, where the average interparticle distance (one-dimensional volume) discontinuously changes from $x = a$ for $P > P_c$ to $x = b$ for $P < P_c$. P_c can be found by the Maxwell construction (dashed inclined line). The one-dimensional model has a region of density anomaly near $T = 0$, $P = P_c$. (b) P - T phase diagram of the shoulder potential for $b = 1.5a$, $c = 2a$, $U_R = 2U_A$ in three dimensions. Thin solid lines are isochores for 12 different densities between $\rho = 0.0492a^{-3}$ and $0.297a^{-3}$, corresponding to the system of $N = 850$ particles in the cubic box with the edge $L = 12.0a$, $L = 12.2a \dots L = 14.2a$. Dashed lines are additional isochores corresponding to $\rho = 0.331a^{-3}$, $0.320a^{-3}$ and $0.317a^{-3}$. Low temperature simulations are hampered by the spontaneous crystallization (indicated by Δ) into a crystal of complex symmetry in which particles separated by hard core distance form parallel lines arranged into a two-dimensional triangular lattice. This crystal melts at much higher temperatures, displaying the melting temperature maximum indicated by ‘ \times ’ symbols. The isochores are interrupted at low temperatures due to increasing relaxation times. The three-dimensional model displays a liquid-liquid phase transition ending at the critical point $T = 0.52U_A/k_B$, $P = 1.05U_A/a^3$ but no density or diffusivity anomaly. It displays the anomalous increase of isothermal compressibility upon cooling for pressures above the thick dashed line, which indicates compressibility minima and maxima as a function of temperature at constant pressure. Above the liquid-liquid critical point we observe a second line of compressibility maxima, which must join with the compressibility minima line at high temperatures. We also observe a line of the isobaric heat capacity maxima (bold solid line), which in the vicinity of the critical point asymptotically coincides with the line of compressibility maxima, forming a Widom line.

which does not have a density anomaly (figure 2(b)) but it does exhibit rich crystal polymorphism [47] and probably polyamorphism. Various smoothening procedures can be applied to the square shoulder and ramp to create a ‘family’ of potentials interpolating between ramp and shoulder [38, 47] which resemble the potential of figure 1. As the ramp potential becomes more and more shoulder-like, the region of density anomaly shrinks until it disappears below the homogeneous nucleation line of the crystalline phase or below the glass transition line.

The extrapolation of the isochores for some purely repulsive soft core potentials below the glass transition or below the crystallization line suggests that some of the isochores might cross at low temperatures that are unachievable in equilibrium simulations (figure 3(b)) [28], indicating the possible existence of the fluid-fluid critical point below the glass transition temperature. However, this critical point does not materialize and the isothermal compressibility and specific heat remain finite on the entire PT plane.

2.5. Shoulder potential with an attractive square well

Adding the attractive part to the potential (figures 4 and 5) causes a negative van der Waals correction $-a\rho^2$ to be added to the equation of state [15]. Thus a high density isochore will be shifted down by a larger value than a low density isochore and therefore shifted isochores may cross at higher temperatures achievable in simulations. Indeed there are soft core potentials

with an attractive part that clearly exhibit two first-order phase transitions, one a gas-liquid transition that ends at a regular gas-liquid critical point, and the other a liquid-liquid transition between two liquids of different densities which ends in an LLC [16, 20] (figures 4(b) and 5(b)). Systems with three or more fluid-fluid critical points have also been observed [25, 45]. For soft core potentials with an attractive part there is a wide range of parameters for which the LLC exists.

Discontinuous square shoulder potentials with an attractive square well (SSSW potentials) have a clear LLC in three dimensions (figure 4) and exhibit a rich crystal polymorphism [20, 21, 26]. The dependence of the critical temperature, pressure and density on the potential parameters is described in [26]. In all of these cases the LLC is metastable with respect to freezing and, although no density anomaly is observed, a compressibility maximum and a heat capacity maximum are observed along the extension of the LLPT line into a supercritical region known as the Widom line [30]. The Widom line is defined as the temperature at which the correlation length achieves its maximum at constant pressure. Alternatively, it can be defined as the pressure at which the correlation length reaches its maximum at constant temperature. These two lines differ far from the critical point, but asymptotically coincide near the critical point where the correlation length diverges. In the vicinity of the critical point, such thermodynamic response functions as compressibility κ_T and heat capacity C_P can be expressed in terms of correlation length. Thus the lines of κ_T and C_P maxima asymptotically coincide with the Widom line.

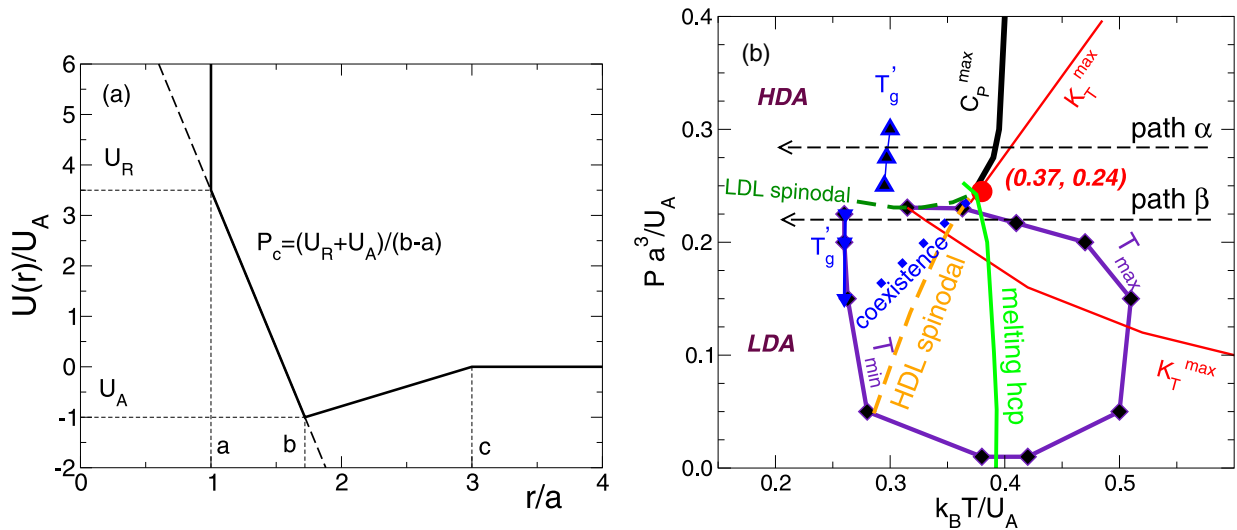


Figure 5. (a) The Jagla potential $U(r)$ (solid line) with an attractive ramp [16]. The potential has two repulsive scales: hard core a and soft core b and an attractive ramp of diameter c . The height of the repulsive ramp is U_R and the depth of the attractive ramp is U_A . If the maximal range of potential $c \leq 2a$, the one-dimensional model has an exact solution which displays a first-order phase transition at $P = P_c = (U_R + U_A)/(b - a)$, $T \rightarrow 0$, where the average interparticle distance (one-dimensional volume) discontinuously changes from $x = a$ for $P > P_c$ to $x = b$ for $P < P_c$. P_c can be found by the Maxwell construction (dashed inclined line). The one-dimensional model has a region of density anomaly near $T = 0$, $P = P_c$. (b) P - T phase diagram of the Jagla potential for $b = 1.72a$, $c = 3a$, $U_R = 3.56U_A$ in three dimensions [37]. It shows a positively sloped liquid-liquid phase transition line ending at the critical point $P_c = 0.243U_A/a^3$, $T_c = 0.373U_A/k_B$, which is located above the equilibrium melting line. Below the critical point is the region of density anomaly, crossed by the line of compressibility maxima/minima which meets the low density liquid spinodal at its minimum. An upper branch of the compressibility maxima, joins the line of heat capacity maxima near the critical point, forming an extension of the coexistence line into the supercritical region (Widom line). The LDL can be studied above the coexistence line, because the HDL phase nucleates only near the LDL spinodal. One can see also the two distinct glass transition lines below which the LDL and HDL transform into respectively LDA and HDA. The region of density anomaly is bounded at low temperatures by the temperature of density minimum, which can be observed in the equilibrium at low pressures but at high pressures it coincides with the glass transition. We perform the differential scanning calorimetry simulations along constant pressure paths α (above P_c) and β (below P_c).

In two dimensions, SSSW potentials may also have a metastable LLCP at some values of the parameters [10, 12, 23], but this question needs further investigation. On the other hand, these potentials have a density anomaly in two dimensions. This density anomaly is associated with freezing into low density, triangular crystals [23] and may be caused by a quasi-continuous nature of the freezing transition in two dimensions: namely by a gradual increase of the characteristic size of the low density crystal-like patches as the melting line is approached [43]. In this example, the density anomaly can be interpreted as resulting from crystal polymorphism, since the patches of local structures resembling a high density square crystal and low density triangular crystal can be clearly identified in the liquid state in the region of the density anomaly [23]. In three dimensions, the solid-liquid transition is sharp and the correlation length remains finite, so no density anomaly is observed. One can expect that square shoulder potentials with an attractive square well could also have distinct glassy states corresponding to different liquid states.

2.6. The Jagla model

The Jagla model is a combination of a repulsive ramp with an attractive ramp (figure 5(a)). The Jagla model has density anomalies and a stable LLPT separating low density liquid (LDL) and high density liquid (HDL) both in two and three dimensions [15, 16]. LDL and HDL have two distinct

glassy states: LDA and HDA (figure 5(b)) [17, 30, 33, 37], which are characterized by two different glass transition (GT) temperatures T_g . Various families of continuous potentials can cover the intermediate scenarios between the Jagla potential and the SSSW potential [38, 39]. The existence of the LLCP and its position—as well as the existence of the density anomaly—strongly depends on the minute features of the potentials. Note that the spherically symmetric potential computed as the inversion of the oxygen-oxygen pair correlation function for water [5, 6], although very similar to the Jagla potential, lacks an LLCP and a density anomaly.

Although the Jagla models are the simplest models of water, they capture most of the anomalous features of the behavior of water including the increase of solubility of small non-polar compounds upon cooling and even cold denaturation of proteins [34]. The only significant difference between the phase diagrams of these models and the hypothetical phase diagram of supercooled water is that Jagla models usually have a positively sloped LLPT coexistence line [16, 30, 42] (figure 5(b)), so that their critical points lie above the region of the density anomaly, while the phase diagrams of classical water models based on Coulomb interactions have a negatively sloped coexistence line, and their LLCP is surrounded by the region of the density anomaly [91, 92]. The reason for this discrepancy is that, in the Jagla model, the HDL has lower entropy than LDL, and hence due to the Clapeyron relation a positively sloped coexistence line.

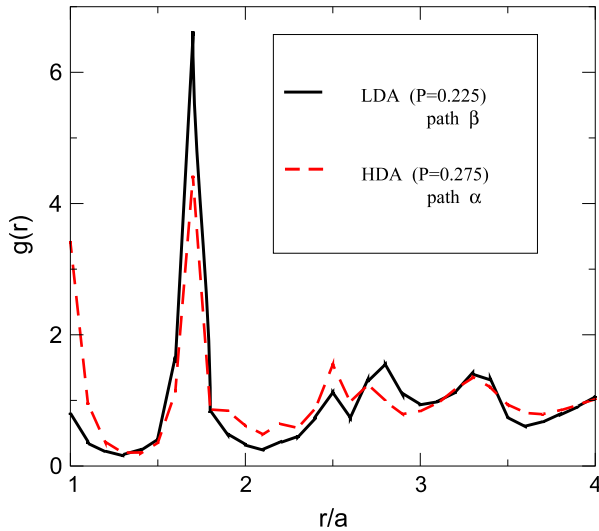


Figure 6. Illustration of the structural difference of the LDA solid and HDA solid by the radial distribution function $g(r)$ for the Jagla model. The LDA solid is obtained upon cooling LDL along path β ($P = 0.225U_A/a^3$). The HDA solid is obtained upon cooling HDL along path α ($P = 0.275U_A/a^3$). Note that, for HDA, particles shift from the soft core distance $r/a = 1.72$ to the hard core distance $r/a = 1.0$, so the peak at $r/a = 1.72$ decreases while the peak at $r/a = 1.0$ increases. Similar graphs characterize the behavior of a generic soft core potential with pressure. As pressure increases, some particles shift from the soft core distance to the hard core distance.

HDL and LDL can be simulated simultaneously at any state point in the region between the two spinodals; hence the difference between their entropies can be explicitly computed by thermodynamic integration around the LLCPC. Moreover we can study the glass transition of both LDL and HDL along the same constant pressure path β which goes below the minimum on the LDL spinodal (figure 5(b)). Figure 7 shows the entropies of LDL, HDL, LDA, HDA and the hcp crystal, into which LDL spontaneously crystallizes if one runs long equilibrium simulations slightly above the glass transition temperature. In fact, the entropy of HDL is so low that the entropy of its glass HDA becomes smaller than the entropy of the low density polymorph which has an hcp structure and a smaller density than LDL. This would be a demonstration of the Kauzmann paradox [93] if the HDL could crystallize into this type of crystal. In reality, HDL in the Jagla model must crystallize into a different type of crystal (presumably rhombohedral) with much higher density and much lower entropy. The entropy of this crystal would always remain lower than the entropy of HDA.

2.7. Density minimum

A model that claims to display water-like characteristics must be able to exhibit a temperature of maximum density. This ability is a striking feature of the Jagla models and the ramp models. What is remarkable is that these models display an even rarer density minimum [28, 37].

This feature has been seen before only in supercooled Te, stable As_2Te_3 [94], some GeTe alloys [95], at the upper limit of experiments for BeF_2 [80], and in

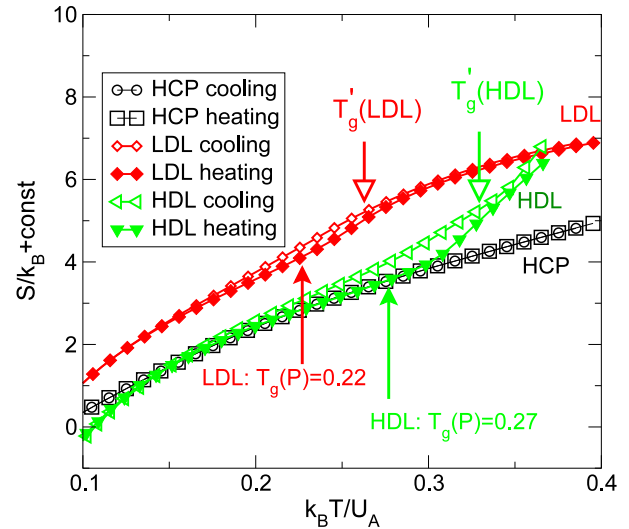


Figure 7. The dependence of the total entropy without the kinetic contribution, $3/2k_B \ln T$, on temperature at constant pressure $P = 0.22U_A/a^3 < P_c$ for the hcp crystal and both types of amorphous states, HDL/HDA and LDL/LDA in the Jagla model. The difference between the entropies of HDL and LDL, $S_{LDL} - S_{HDL} = 1.32k_B$ at $T = 0.32$, is computed by thermodynamic integration around the critical point. The entropy difference between LDL and hcp is $\Delta S = \Delta H/T_m = 2.1k_B$, where $\Delta H = 0.73U_A$ is the enthalpy of fusion and $T_m = 0.345U_A/k_B$ is the equilibrium melting temperature of the hcp crystal into LDL at $P = 0.22U_A/a^3$. The entropy undetermined constant is the same for hcp, LDL and HDL. The difference between the entropies measured upon cooling and heating is caused by the ergodicity break at the glass transition. In all cases the heating/cooling rate is $q_2 = 2 \times 10^{-5} \sqrt{U_A^3/m a^2 k_B^2}$.

the simulations of water [91, 92]. Very recently, the density minimum was observed in laboratory water in very low temperature measurements using noncrystallizing nanoconfined water [96, 97] and in silica [98].

In the Jagla model, the density maximum is always an equilibrium property, but the density minimum is only seen in the equilibrated liquid at the lowest pressures of the existence of the density anomaly at which the density minimum merges with the density maximum. At higher pressures the density minimum is pre-empted by inevitable crystallization in the ramp model (figure 3(b)) or by the GT in the Jagla model (figure 8) for sufficiently high cooling rates at which the crystallization is avoided. For slower cooling rates the minimum would presumably continue as an equilibrium phenomenon. There is an apparent density minimum near GT because the glassy state has a positive thermal expansion coefficient.

Figure 8 shows how the two extrema, T_{\min} and T_{\max} , merge at low pressures and would also merge at higher pressures except for the phase change to HDA caused by an intersection with the LDL spinodal. According to the theorem proved in [99], the temperature of the density maximum line meets the LDL spinodal at the point of its minimum on the P - T plane. Moreover, the slope of both curves at the point of their intersection must be equal to zero. Figure 5(b) is in complete agreement with these statements. No density anomaly is observed above the critical pressure upon crossing the Widom

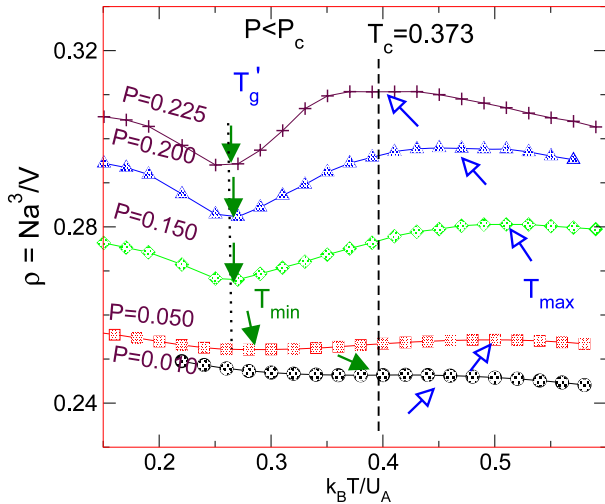


Figure 8. Demonstration of the effect of the GT on density minimum along path β for $P < P_c$ in the Jagla model. For relatively high pressures below P_c ($0.05U_A/a^3 < P < P_c$), the density minima are located near the GT temperature T'_g along different paths. For low pressures $P < 0.050U_A/a^3$, the T_{\min} is located in the ergodic region, and at $P \approx 0.01$ it approaches the temperature of maximum density T_{\max} . The T_{\max} line (open arrows) and the T_{\min} line (filled arrows) confine the density anomaly region which disappears near the critical point and at very low pressure.

line. Therefore, the T_{\min} and T_{\max} are not caused by the Widom line in the Jagla model. The line of κ_T maxima coincides with the Widom line near the critical point, but it forms a large loop in the P – T plane, crosses the T_{\max} line at the point of its maximal temperature, and then turns upwards to cross the T_{\max} line at its ending point, where they both meet the LDL spinodal. As mentioned above, this special point is a minimum of the LDL spinodal and a maximum of the T_{\max} line. It is also the common intersection of the LDL spinodal, the T_{\max} line, and the compressibility maxima line.

The situation is quite different in the ST2 and TIP5P models of water [91, 92] in which the LLPT coexistence line and the Widom line have negative slopes. In this case the critical point lies in the region of the density anomaly and the T_{\max} line enters the HDL region and meets the HDL spinodal at the point of its maximal pressure. The compressibility maximum line goes down from the critical point along the Widom line, crosses the T_{\max} line at the point of its maximal temperature, makes a large loop on the P – T plane, encircles the critical point at high pressures and crosses the T_{\max} line at the HDL spinodal maximum. These examples show that the existence of T_{\min} and T_{\max} are always associated with the line of compressibility maxima that passes through the region of the density anomaly bounded by these two lines, but the Widom line does not necessarily lie in this region.

Gibson and Wilding [42] have studied a family of Jagla potentials by gradually reducing the range of both the repulsive and attractive ramps. Accordingly, the slope of the coexistence line decreases but the LLCPP shifts to lower temperatures and eventually disappears below the line of crystal homogeneous nucleation. At this point, the coexistence line acquires a slightly negative slope, but this is within the error bars.

We can expect this negatively sloped LLPT coexistence line to continue into the supercritical region as the Widom line [30] with a negative slope. Thus we can expect that, in the case of a negatively sloped coexistence line, the Widom line will go from a critical pressure to zero pressure as the temperature increases. The critical density fluctuations associated with the κ_T maximum and diverging correlation length ξ may induce crystallization into a low density solid whose local structure is similar to that of low density liquid (LDL). Hence one can expect that, in the case of a negatively sloped LLPT line, the homogeneous nucleation line coincides with the Widom line. This is hypothesized to be the case for water [100]. If the coexistence line has a negative slope, the entropy of the LDL is lower than the entropy of the high density liquid (HDL) due to the Clapeyron equation. Thus the LDL may serve as an Ostwald step on the way to a low density crystal. Similar features are exhibited by the Molinero monatomic water model based on the Weber–Stillinger three-body potential [76].

When the coexistence line is positively sloped, the domain of LDL can be entered along a constant pressure path below the LLCPP without entering a region of large density fluctuations (figure 5(b)). In this case, the low density branch of the line of compressibility maxima also runs through the region of the density anomaly, crossing the temperature of the maximum density line at its maximal temperature [99], but the compressibility remains small and does not diverge as it does in the vicinity of LLCPP. The low density branch of the compressibility maxima line does not reach the LLCPP but may cross the LLPT coexistence line and join the LDL spinodal at the point of its minimum, or exit the region of the density anomaly through the point of the minimal temperature on the minimal density line. Thus, for the positively sloped LLPT coexistence line, one can enter the LDL domain below the critical pressure without crossing the region of high density fluctuations and hence avoiding crystallization. Another interpretation of the stability of the LDL in the case of the positively sloped LLPT coexistence line is that the LDL is significantly more disordered than HDL and hence it is separated from the low density crystal by a high entropic barrier. The HDL is less prone to crystallization because its density and entropy are still much higher than the density and the entropy of the high density crystal. Accordingly, in the case of the positively sloped LLPT coexistence line, the LLPT is usually stable with respect to crystallization. Therefore, the Jagla model is the ideal model to study polyamorphism in the glassy state and polyamorphism in relation to the liquid–liquid transition. After appropriate parameterization it may also be applied to the study of metallic glasses [37].

2.8. Differential scanning calorimetry (DSC) of the Jagla model

Here we discuss in some detail recent studies [37] of the interplay of the glass transition and the liquid–liquid phase transition in the Jagla model. Our results are based on discrete molecular dynamics (DMD) simulations [101] of the Jagla model [15] defined in figure 5(a). A common experimental

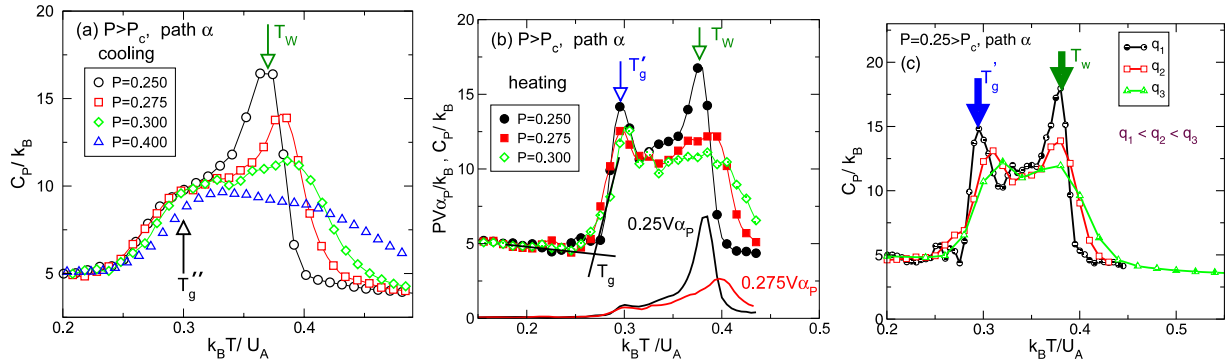


Figure 9. Demonstration of glass transitions in HDL by comparing the T dependence of C_P on cooling and heating in the Jagla model. (a) Cooling HDL along path α and (b) heating HDA along path α at different pressures $P > P_c$. Upon cooling, C_P shows a maximum at $T = T_W$ and a shoulder at $T_g'' \approx 0.3U_A/k_B$, below which the liquid vitrifies to HDA. In contrast, upon heating HDA, C_P shows a peak at T_g' , characterizing the GT and corresponding to the shoulder found upon cooling in (a). The standard construction denoted by the dashed straight lines indicates that the GT temperature is $T_g \approx 0.27U_A/k_B$ for all the pressures studied. Further heating results in a second peak at the Widom line, $T = T_W$. While T_g is nearly constant at $P > P_c$, the Widom line temperature T_W shifts to higher values as P increases. Moreover, due to critical fluctuations as $P \rightarrow P_c$, the height of the Widom line peak is much more sensitive to P than that corresponding to the GT. We use a slow cooling rate of q_1 , since crystallization is not observed for $P > P_c$. We also show $PV\alpha_P$, the volumetric contribution to C_P . We see a small peak in α_P which occurs at T_g' and a large peak which occurs at T_W . This peak makes a principal contribution to the C_P peak at Widom line. (c) Heating the glass along path α ($P > P_c$ very close to P_c) with different heating rates $q_1, q_2 = 2q_1$ and $q_3 = 4q_1$. As the heating rate increases, the GT peak at $T = T_g'$ shifts to higher temperature as expected. In contrast, the Widom line peak does not shift with the heating rate; instead it becomes wider and less sharp as q increases, but the total area under it does not change. In summary, we demonstrate that the GT peak is not sensitive to P but is sensitive to heating versus cooling, while the Widom line peak, which is almost entirely due to the volumetric contribution, is sensitive to P but not to heating versus cooling. In contrast the GT peak is sensitive to the heating rate, while the Widom peak is not sensitive to the heating rate except in the close vicinity of the LLCP.

technique for studying the GT is DSC, which detects the GT by a maximum in C_P upon heating the glass back to the liquid state. A maximum in C_P also occurs in systems with LLPT. The corresponding maxima, obtained at different pressures in the supercritical region, form a line that, as the LLCP is approached, becomes the Widom line. Some systems, such as the Jagla model, present both the GT and LLPT. Here we ask (i) how the GT and LLPT would be detected in DSC experiments and (ii) if the GT and LLPT are related.

An important parameter of the DSC experiments is the cooling/heating rate, q . In [37] three heating rates were studied, $q_1, q_2 = 2q_1$ and $q_3 = 4q_1$, where $q_1 = 10^{-5} \sqrt{U_A^3/ma^2k_B^2} \approx 7 \times 10^9 \text{ K s}^{-1}$ if one uses the values a, U_A and particle mass m , to fit the water behavior. This value is four times smaller than the one used in SPC/E simulations of water [102].

Cooling the HDL along constant pressure path α at $P > P_c$ (figure 5(b)) results in the HDA glass. We do not observe any spontaneous crystallization along path α even at the slowest cooling rate q_1 . This path crosses first the line of C_P maximum at T_W associated with the Widom line. Figure 9(a) demonstrates the behavior of C_P along such paths for several pressures. The structural changes from the LDL-like liquid above T_W to the HDL-like liquid below T_W are associated with a rapid decrease of diffusivity, which resembles the behavior of fragile liquids [30, 33]. Note that the position, height and shape of the Widom peak strongly depends on pressure. While near the critical point the peak is very sharp and almost diverging as expected, at high pressures far away from P_c the peak becomes very broad and shallow and practically disappears at $P = 0.4U_A/a^3$. Note that at high temperatures $T > T_W$, C_P

increases with pressure as the path shifts away from the critical pressure. A similar effect can be seen for water in which the heat capacity also decreases as the constant pressure path approaches the hypothetical critical point value $P \approx 200 \text{ MPa}$ for $T > -25^\circ\text{C}$ [103]: the Widom peak becomes broad enough to be seen at $P = 0.1 \text{ MPa}$, but might be very narrow and might shift to lower temperatures at $P = 150 \text{ MPa}$, so that no heat capacity increase associated with it can be detected. The only difference is that in water the Widom line presumably has a negative slope and thus must be detected below P_c .

As the temperature drops further, C_P starts to decrease again due to the loss of ergodicity and forms a characteristic shoulder at $T = T_g'' < T_W$, which almost does not depend on pressure. Near T_g'' the diffusivity changes its behavior and starts to follow an Arrhenius law which is a characteristic of strong liquids. Thus we can relate the fragile behavior with crossing the Widom line, while we can relate the strong behavior with the glass transition. As C_P reaches the plateau below GT, the liquid turns into the HDA solid, whose structure is characterized by the peak of the RDF at the hard core distance a (figure 6). Each particle in the HDA has approximately 1.8 neighbors in the first coordination sphere. In the monatomic solid, C_P must reach the Dulong–Petit value of $3k_B$. However, due to discontinuity of the potential in the discrete molecular dynamics, which has a characteristic step of $U_A/8$, this limiting value is not reached. Variants of the Jagla model which employ continuous potential [17, 38] or potentials with smaller steps [28] would eliminate this problem.

As we heat the HDA back (figure 9(b)), C_P produces a characteristic overshoot at $T_g' \approx T_g''$, indicating the restoration

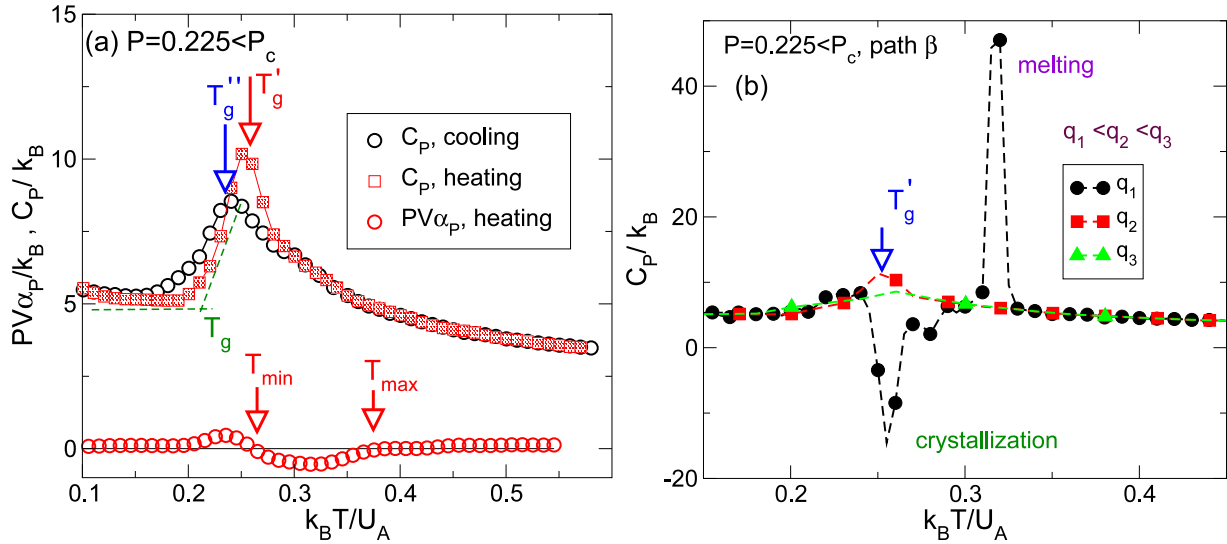


Figure 10. Demonstration of glass transitions in LDL by comparing the T dependence of C_p on cooling and heating in the Jagla model. (a) Cooling LDL along path β for $P = 0.225U_A/a^3 < P_c$. C_p increases and shows a maximum at $T_g'' \approx 0.24$; further cooling results in an LDA glass. Upon heating LDA along path β , a sharp increase in C_p occurs as $T = T_g$ and C_p displays a maximum at $T_g' \approx 0.26U_A/k_B$. The standard construction denoted by the dashed straight lines indicates that, at the present pressure, the GT temperature is $T_g \approx 0.22U_A/k_B$. We use a fast cooling or heating rate, q_2 , to avoid crystallization. We also show the behavior of $PV\alpha_p$, the volumetric contribution to the C_p . We see that anomalous behavior ($\alpha_p < 0$) switches to normal behavior ($\alpha_p > 0$) in the vicinity of T_g' . (b) Heating the LDA along path β ($P < P_c$) at different cooling rates. At faster heating rates $q = q_2$ and q_3 no crystallization occurs and the behavior of C_p near GT is the same as for $P > P_c$, i.e. the T_g' peak shifts to higher temperatures and becomes less pronounced as the heating rate increases. For a low heating rate $q = q_1$ crystallization into the hcp crystal occurs just above the glass transition at T_g . As a result the peak at T_g' is almost completely suppressed by the latent heat release associated with rapid crystallization. Since the enthalpy of the crystal which grows as the temperature increases is less than the enthalpy of the glass, we see an apparent specific heat minimum at $T = 0.25U_A/k_B$. This situation is very similar to what occurs at the experimental GT in water [107] at low pressures. The hcp crystal melts upon further heating and produces an endothermic peak in C_p at $T = T_m = 0.32U_A/k_B$. Note that the ratio of the GT temperature $T_g = 0.22U_A/k_B$ and the melting temperature T_m is $2/3$, thus mimicking the classical glassformer value $2/3$ due to Kauzmann [93].

of ergodicity associated with the glass transition. The position and the height of this peak is almost independent of pressure. In contrast, the behavior of the Widom peak is the same upon heating as upon cooling, provided the heating/cooling rate is slow ($q \geq q_1$). This means that the Widom peak is the equilibrium feature of the liquid phase. The value of the GT temperature $T_g < T_g'$ can be found by a standard construction [104], indicated by the crossing of straight lines fitting the slope of the peak and the plateau.

Another experimental method of detecting a glass transition is to measure the thermal expansion coefficient α_p as a function of temperature [105], which must produce a characteristic overshoot at T_g' upon heating. Figure 9(b) also shows $PV\alpha_p$, the volumetric contribution to C_p for $P = 0.25U_A/a^3$ and $P = 0.275U_A/a^3$ (black and red solid lines, respectively). Indeed, we see a small peak at T_g' followed by a large peak at T_W . This result suggests another experimental technique, which clearly distinguishes the Widom line from the GT. As we cross the Widom line, the volume of liquid must dramatically change with temperature due to structural changes in the liquid transforming from the HDL-like to the LDL-like states. Accordingly α_p must produce a large peak. The height of this peak must diverge near the critical point. In contrast the GT peak in α_p must be small and must not depend on pressure, because the structural changes associated with GT are minor. Note that for water, in which the Widom line has a negative

slope, the high temperature phase is HDL-like, thus we would expect a diverging negative peak in α_p near the Widom line, followed by a small positive peak at T_g' .

Finally, an important distinction between the Widom line and the GT is given by the heating rate dependence of the correspondent peaks (figure 9(c)). As the heating rate decreases, the glass transition peak becomes more prominent and shifts to the lower temperatures, which is qualitatively consistent with experimental results [106]. The Widom line peak at $T = T_W$ in principle should not depend on the heating rate. However, along $P = 0.25U_A/a^3$, which is very close to P_c , the magnitude of the Widom line peak decreases when the heating rate is rapid. This is due to the critical slowing down of dynamics near the LLC. Nevertheless, the position of the peak at T_W and the total area under it (corresponding to the enthalpy gain) do not change with the heating rate.

In the Jagla model, the LLPT coexistence line has a positive slope. Therefore below the critical pressure, path β crosses the coexistence line, instead of the Widom line. The coexistence line produces no effect on the behavior of the LDL which can be supercooled below the coexistence line without nucleation of the HDL. The particular shape of the LDL spinodal (which has a minimum) guarantees that, for $P < 0.23U_A/a^3$, the LDL remains metastable in the entire temperature range and it can undergo a glass transition without forming HDL provided the heating/cooling rates are

fast enough ($q \geq q_2$) so that crystallization does not occur. Figure 10(a) shows the C_P behavior for cooling and heating along path β . The behavior at GT is qualitatively similar to that for $P > P_c$, except that no Widom peak is observed. The values for T_g , T_g' and T_g'' has the same meaning as for $P > P_c$ but has much smaller values. The diffusivity changes along path β in a non-Arrhenius way characteristic for fragile liquids and becomes undetectable in the computer simulations for $T < T_g$. The thermal expansion coefficient α_P is negative in the region of density anomaly between the temperature of minimal density, $T_{\min} \approx T_g'$, and the temperature of maximum density, T_{\max} . For this pressure, T_{\min} is not the equilibrium property of liquid, but is associated with the GT, because, as the majority of solids, the glass must have $\alpha_P > 0$. Upon heating between T_g and T_g' , α_P develops a small overshoot followed by a small undershoot, associated with the restoration of ergodicity upon heating. This result shows that it is not easy to distinguish the true equilibrium T_{\min} from the one associated with GT. Additional calorimetric information must be taken into account.

Upon heating LDA along path β at $P < P_c$, the heating rate has drastic effects on C_P (figure 10(b)). In particular, heating LDA above T_g at a slow rate $q = q_1$ results in crystallization. At this slow rate, the particles have sufficient time to form crystal nuclei. Thus the system spontaneously crystallizes into the hcp crystal, which has a lower free energy than the metastable liquid. This crystallization is associated with the release, upon heating, of latent crystallization heat resulting in an apparent negative peak in C_P . Upon further heating, the crystal finally melts at the melting temperature $T_m = 0.32$, indicated by a strong endothermic peak in C_P . Crystallization events are not observed upon heating at faster rates. The behavior of C_P at a slow heating rate (i.e. a GT peak followed shortly by a crystallization peak and then by a melting peak) is very similar to that observed in the DSC experiments of [107], obtained upon heating glassy water at atmospheric pressure. We note that the peak associated with the GT observed at $q = q_1/2$ and $q = q_1/4$ is barely observable at $q = q_1$ due to the onset of crystallization.

2.9. DSC simulations of the ramp model

As we see, the DSC simulations of the Jagla model give us useful insights on how the LLPT can be observed in the presence of the GT. The problem here is that the entropy of the HDL is lower than the entropy of LDL which is the opposite to the situation in water. Therefore, it is interesting to investigate the ramp model (figure 3(a)), in which the LLCP is submerged below the glass transition, but still we can expect to have two types of glasses, HDA and LDA. In this model, the region of density anomaly is wider than in the Jagla model. Hence the entropy increases upon compression for a wider range of pressures, almost up to the pressure of the hypothetical LLCP. Therefore we can expect that the entropy of HDA in this model will be higher than the entropy of LDA. Accordingly, we can expect that the Widom line emanating from this hypothetical LLCP will have a negative slope and might enhance the crystallization rate at low pressures, which

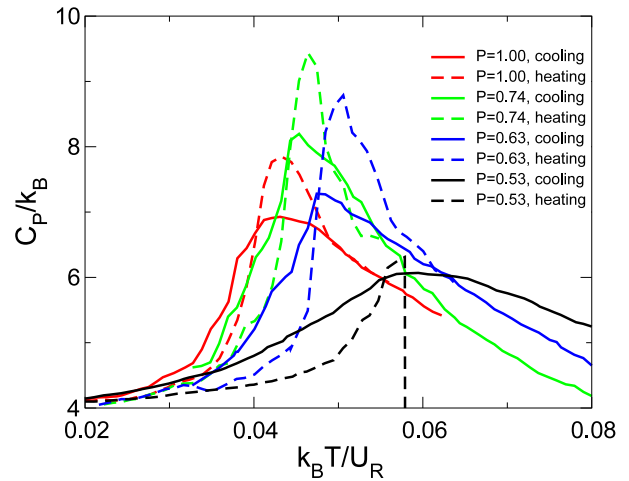


Figure 11. The behavior of C_P upon heating and cooling along the constant pressure paths for the ramp model. Each curve has a single maximum, the position of which coincides upon heating and cooling, which means that no Widom line is observed. Note that the peaks are getting sharper and higher close to the pressure of the hypothetical critical point and that the GT rapidly shifts to high temperatures as the pressures decreases from $P = 0.6U_R/a^3$ to $P = 0.5U_R/a^3$. Thus we can classify the glasses for $P \geq 0.6U_R/a^3$ as HDA while the glass for $P = 0.5U_R/a^3$ as LDA. However no sharp distinction is possible. The entropy of LDA glass is smaller than the entropy of the HDA glasses, which can be seen from a large value of C_P in the case of LDA. Note that the heating of the LDA is associated with crystallization (an abrupt drop of C_P at the end of the heating curve) even for the fastest heating rate we study.

has indeed been observed in [28]. Moreover, the presence of this Widom line will result in larger heat capacity peaks along path β . All this makes the situation in the ramp model more similar to that in water. Thus it would be instructive to repeat the DSC simulations for this model, in order to see if the Widom line could be distinguished from the GT.

Figure 11 shows the behavior of C_P along several constant pressure paths. We can clearly see that along all these paths there is only one peak in C_P , and that the overshoot upon heating occurs exactly on top of the cooling peak. Hence no separate Widom peak is observed. This means that no direct evidence of the LLPT can be obtained, although the magnitude of the peaks increases as we approach the pressure of the hypothetical critical point, $P \approx 0.8U_A/a^3$ (see figure 3(b)). The DSC experiments in the nanoconfined water will show whether or not water has a Widom peak separated from the GT peak.

In the ramp model, it is difficult to characterize the situation as the true polyamorphism, although the structures of the LDA and HDA obtained at different pressures have the same qualitative difference as the structures of HDA and LDA in the Jagla model (figure 6), in which the polyamorphism is true and the glass transitions in HDA and LDA can be studied at the same pressure (figure 7) resulting in the different GT temperatures and different behavior of the diffusivity [33, 37]. In the ramp model, the HDA glass recovered at lower pressure gradually transforms into the LDA before the glass transition. The compression–decompression simulations of the ramp model performed at

very low temperatures result in the hysteretic PV curve with a portion of high compressibility but no true instability [17]. In contrast, the low density hcp crystal collapses into HDA, in an abrupt transition as in water experiments [62]. Moreover, in the Jagla model, where the true polyamorphism exists, the LDA collapses into HDA in an abrupt transition similar to the hcp collapse, and HDA explodes into LDA, almost in the same way as HDL and LDL interconvert at their spinodals [33]. In summary, we can expect, that in experiments there will be an entire spectrum of situations with different degrees of polyamorphism, starting from a sharp first-order-like transition as between HDA and LDA water and ending in a gradual transition such as between HDA and very high density amorphous ice (VHDA) [108, 109].

3. Anomalous melting behavior

In a typical simple fluid, the fluid–solid coexistence line runs monotonically to higher temperatures when the pressure is increased. An example of this behavior is provided by a system of particles interacting through the Lennard-Jones potential, which is the most successful model for simple, argon-like, fluids. At low pressures most substances exhibit a similar fluid–solid coexistence line. At higher pressures a number of elements undergo a radical change: the melting line passes through a maximum and enters a region of re-entrant melting, i.e. a region where melting occurs when the pressure is increased and the temperature kept constant. If the pressure is further increased, the melting line may recover a positive slope (e.g. Cs, Rb, Na, Ba, Te, etc) [110]. As advances in experimental methods make it possible to reach higher pressures, it has been found that an increasing number of substances show a non-monotonic melting line. Such melting behavior is often called ‘anomalous’ to point out that it differs from the monotonic standard (i.e. similar to the Lennard-Jones fluid) behavior. Re-entrant melting is relevant also in a completely different context, i.e. for soft matter. Pair interactions with a soft repulsive component, used for modeling such systems as star polymers, microgels and colloidal suspensions [111], have been shown to exhibit re-entrant melting behavior, often in association with water-like anomalies [112]. The occurrence of similarities in the melting behavior of substances with apparently antithetical features, such as atoms, traditionally assumed to be ‘hard’ objects, and soft matter, surprising as it may appear, is related to the softening effect that extremely high pressures may exert on interparticle repulsive interactions.

One classical potential that is widely used to calculate the equation of state of materials under extreme conditions is the exp-6 potential [113]:

$$u(r) = \begin{cases} +\infty, & r < \sigma_M \\ \frac{\epsilon}{\alpha - 6} \left[6 e^{-\alpha(r/\sigma - 1)} - \alpha \left(\frac{\sigma}{r} \right)^6 \right], & r \geq \sigma_M \end{cases} \quad (9)$$

where r is the interparticle distance, ϵ is the depth of the attractive well, σ is the position of the well minimum, α (usually taken in the range 10–15 [114]) controls the steepness

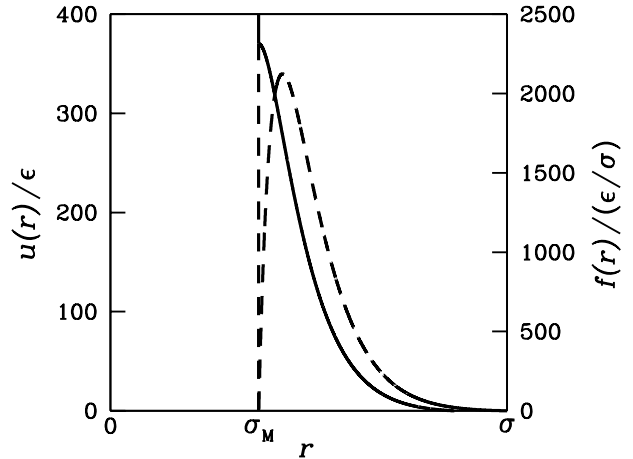


Figure 12. The exp-6 pair potential $u(r)$ (solid line, left vertical axis) and the corresponding force (dashed line, right vertical axis). With increasing α , σ_M decreases while $\epsilon_M = f(\sigma_M)$ increases (for variation between 11 and 13, σ_M and ϵ_M vary in the range $0.374\sigma - 0.245\sigma$ and $370\epsilon - 7104\epsilon$, respectively).

of the exponential repulsion and σ_M is the point where the function in the second line of (9) attains its maximum value ϵ_M . The relative softness of the repulsion described by the exp-6 potential has long been known, but only recently has its soft nature been fully recognized [115]. In fact, the exp-6 interaction exhibits a region of downward concavity in its repulsive component; hence it is characterized by the existence of a range of interparticle distances where the repulsive force $f(r) = -du(r)/dr$ decreases as two particles get closer to each other (figure 12). This constitutes the origin of two separate repulsive length scales: (i) a larger one corresponding approximately to the local maximum of the repulsive force and (ii) a smaller one associated with the hard core diverging repulsion.

We calculate, using Monte Carlo numerical simulation, the exp-6 phase diagram in the PT (pressure–temperature) plane for $\alpha = 11$ (figure 13). We perform calculations using NPT Metropolis Monte Carlo in conjunction with Widom and Frenkel–Ladd free-energy methods [116]. The number N of particles in the samples considered is of the order of 1000 (performing checks with larger samples as a test for finite-size corrections and finding them to be negligible). In what follows, the pressure P and temperature T are expressed in units of ϵ/σ^3 and ϵ/k_B , respectively. The fluid–solid coexistence line starts at low P with a positive dT/dP slope that gradually decreases with increasing pressure until it vanishes at a point of maximum melting temperature T_M . This is followed by a pressure interval in which the slope is negative. Eventually, at extremely high pressures, the melting line recovers a positive slope. When increasing pressure at a fixed temperature smaller than T_M , the system, initially fluid, becomes increasingly dense until it crystallizes. Below a given temperature (≈ 10), the system crystallizes first into a face-centered cubic (fcc) structure and then, upon increasing pressure further, undergoes a transition into a body-centered cubic (bcc) solid. This effect is related to a decrease in the mean nearest-neighbor distance when the pressure is increased, which causes particles to enter

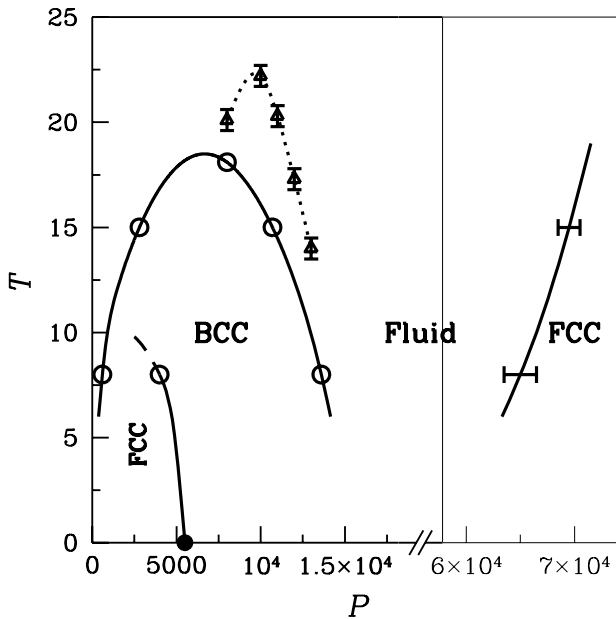


Figure 13. Phase diagram in the PT plane of the exp-6 interaction model for $\alpha = 11$. Pressure P and temperature T are expressed in units of ϵ/σ^3 and ϵ/k_B , respectively. Coexistence curves are represented as solid lines. Open circles represent coexistence points as estimated through exact free-energy calculations (errors are smaller than the size of the symbols). The full circle is obtained through an exact classical total-energy calculation. The boundary between the fluid phase and the FCC crystal at extremely high pressures corresponds to the lower stability threshold of the solid. The locus of density maxima $(\partial\rho/\partial T)_P = 0$ (temperature of maximum density line) is represented as a dotted line. All lines in the figure are guides for the eyes. Data are from [115]. In the intermediate-pressure region (between the low density solid and the extremely high density one) additional solid phases are presumably present at low temperature as suggested from the calculation of the chemical potential at zero temperature (see text).

inner, less steep regions of the interaction potential. As the pressure is further increased, this solid undergoes re-entrant melting into a denser fluid. This is a consequence of the increasing competition between the two scales of the first-neighbor distance. The larger length scale, associated with the soft repulsion (effective at the lower pressures), loses effectiveness, as pressure increases, in favor of the smaller length scale related to the particle core diameter σ_M (dominant at the higher pressures). Eventually, at very high pressures, the fluid crystallizes into a hard-sphere-like fcc solid.

The above interpretation is corroborated by an analysis of the structural properties of the exp-6 system. We compute the radial distribution function $g(r)$ and the structure factor $S(k)$ at a temperature T close to T_M for several pressures, in the pressure range where re-entrant melting occurs. Upon compression, the first peak of $g(r)$ (at $r = \sigma_M$) moves upward while the second and third peaks go down, signaling that an increasing number of particles are overcoming the soft repulsive shoulder (figure 14). This behavior is mirrored in the pressure dependence of $S(k)$, whose main peak first builds up, signaling ordering (in the pressure range where, at lower temperatures, the fluid crystallizes into a low density solid), and then goes down as the system becomes increasingly

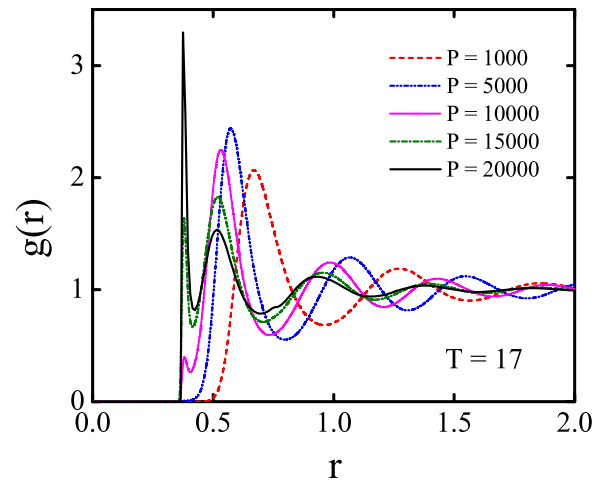


Figure 14. Pair distribution function $g(r)$ of the exp-6 interaction model for $\alpha = 11$. $P = 1000$ (dashed line), 5000 (double dotted-dashed line), 10 000 (dotted line), 15 000 (dashed-dotted line) and 20 000 (solid line).

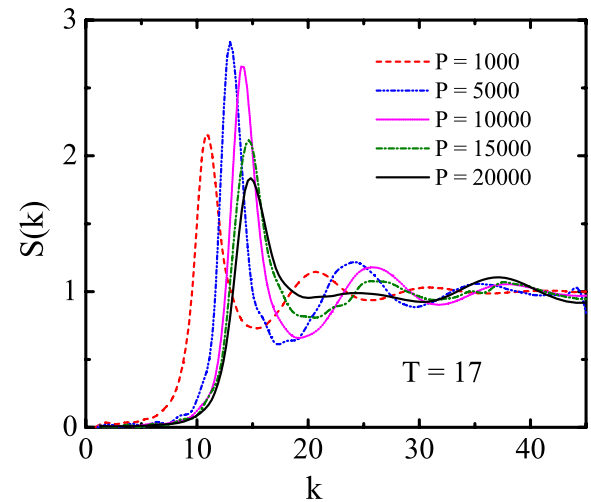


Figure 15. Structure factor $S(k)$ of the exp-6 interaction model for $\alpha = 11$. $T = 17$; $P = 1000$ (dashed line), 5000 (double dotted-dashed line), 10 000 (dotted line), 15 000 (dashed-dotted line) and 20 000 (solid line).

disordered (figure 15). The behavior of $g(r)$ and $S(k)$ is consistent with disappearance of the soft repulsive length scale as the pressure is increased (leaving the hard repulsive length scale), and is completely different from the behavior characterizing simple fluids, where all the peaks of $g(r)$ and $S(k)$ increase as P increases at constant T .

In the large pressure range between low density and extremely high density solids, we may expect the exp-6 system to form different solid phases at low temperatures. The possible solid structures can be anticipated by calculating at zero temperature the chemical potential (i.e. enthalpy) for a number of relevant crystal lattices. We examine a large number of potentially relevant structures including, among the possible candidates, all Bravais crystals as well as a number of non-Bravais lattices (i.e. Bravais lattices with a basis) that have shown themselves to be relevant for some soft material

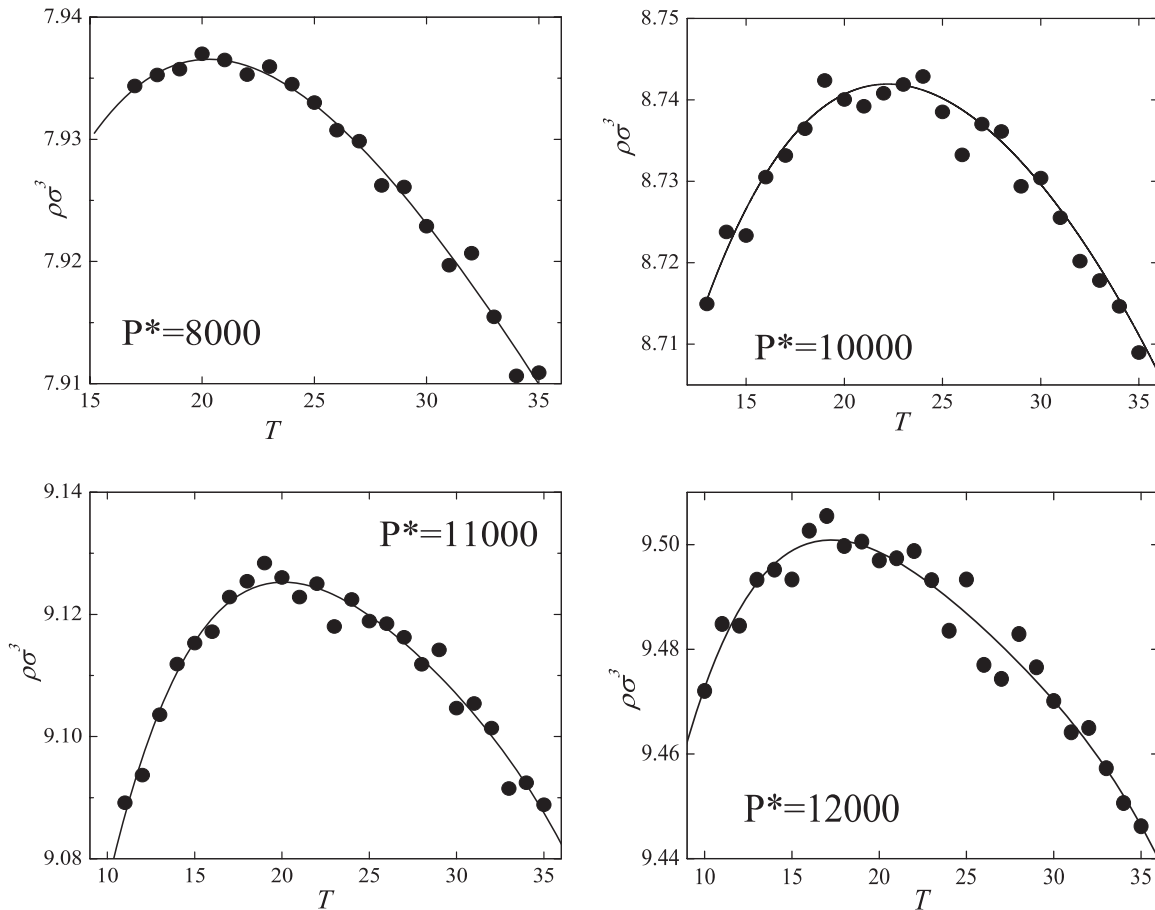
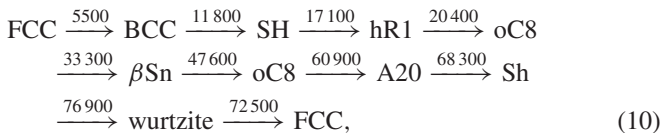


Figure 16. Reduced number density as a function of temperature for $P = 8000, 10\,000, 11\,000$ and $12\,000$ (full dots). All lines are fourth-order polynomial fits of the data points.

or simple substance under high pressures. We find that the sequence of stable crystals for increasing pressures is [117]



where the numbers above the arrows indicate the transition pressures (to within an accuracy of 100). The symbols sh and hR1 are simple hexagonal and simple rhombohedral lattices, oC8 is the structure of αGa , the βSn lattice occurs also for Si, Ge, Rb and Cs and A20 is an orthorhombic lattice providing the structure of αU , βGa and γTi . Our results show that non-Bravais lattices can represent the stable structures also for simple spherically symmetric classical interactions. The extremely rich polymorphism of the exp-6 system with respect to Lennard-Jones-like potentials follows from the fact that in these last systems the fcc and bcc crystals allow us to accommodate second and third neighbors at convenient distances. On the other hand, in systems interacting through softened core potentials, fcc and bcc local orders are destabilized by the peculiar dependence of the interatomic force with distance, which leads to the existence of two incommensurate length scales that frustrate very compact arrangements. The existence of two competing repulsive length scales appears then to be an essential ingredient if

‘exotic’ structures are to represent in some range of pressure the stable phase for isotropic interactions. Our results are relevant not only for atomic systems at high pressures, but indicate also that suitably tailored colloids may exist in such solid phases under standard conditions.

The anomalous melting behavior of the exp-6 system is associated with the water-like anomalous behavior of the number density. If temperature is decreased and pressure is kept constant, in the fluid region above the re-entrant portion of the melting line the density first increases and then, contrary to its usual behavior, decreases (figure 16). The region in which the density exhibits anomalous behavior is delimited by the temperature of the maximum density line that coincides with the locus of points where the density attains its maximum value (figure 13). The decrease of density follows from open local structures being favored over compact local structures as the temperature is decreased. This density anomaly has been observed in a number of substances, among which water is the most relevant [118, 119], as well as in model systems characterized by a soft repulsion. Concerning model systems, it is to be noted that the presence of a re-entrant region in the melting line is not necessarily associated with density anomaly. For example, the square shoulder and SSSW potentials undergo re-entrant melting (see figures 2 and 4) with no density anomaly.

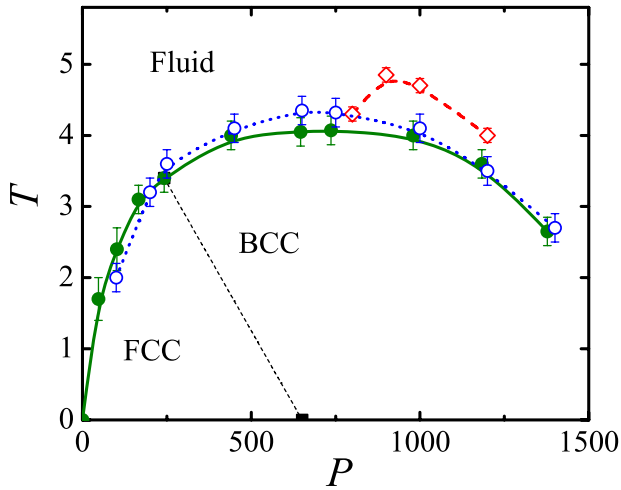


Figure 17. Phase diagram in the PT plane of the exp-6 interaction model for $\alpha = 10$. Pressure P and temperature T are expressed in units of ϵ/σ^3 and ϵ/k_B , respectively. Melting points (calculated through the Lindemann criterion) are represented as full green dots. A rough estimate of the boundary between the bcc and fcc solids (black dotted line) is obtained by drawing a straight line from the full square at $T = 0$ (following from an exact total-energy calculation) to the point on the melting curve where the value of the Lindemann ratio switches from 0.15–0.16 (fcc) to 0.18–0.19 (bcc) [128, 129]. We also plot the fluid–solid coexistence locus as obtained by the heat-until-it-melts criterion (blue open dots), which agrees well with the Lindemann-based estimate. The locus of density maxima in the fluid phase is marked by red diamonds. All lines in the figure are guides to the eyes. Data are from [130].

In order to analyze how the phase behavior of the exp-6 model changes with the steepness of the repulsion, we calculate the phase diagram for $\alpha = 10$ (see figure 17). We find that the overall shape of the melting line is similar to that of $\alpha = 11$, but the anomalous features (i.e. the maximum in the melting line and the following re-entrant melting region, as well as the region of anomalous density behavior) occur at much lower pressures and temperatures. By performing calculations for other values of α in the range 10–13, we find that the maximum melting temperature T_M and the corresponding pressure P_M approximately scale as $\epsilon_M(\alpha)/\sigma_M(\alpha)^3$ and $\epsilon_M(\alpha)$, respectively. This is a sensitive dependence, since a unitary increase (in the interval considered) implies approximately a tenfold increase of P_M and a fivefold increase of T_M .

Analyzing the melting behavior of the exp-6 system may help us understand the anomalous features that characterize the melting of many materials under extreme conditions. It is known that pressure can trigger a reorganization of atomic structure. This can lead to a number of phenomena such as charge transfer to more localized orbitals (e.g. the 6s–5d transition in Cs [120]), orbital hybridization (e.g. the 5p–5d one in Xe [121]) or, more generally, a collective response of conducting electrons creating, upon compression, a more compact crystal lattice. The transition of an element to a more compact solid is usually reflected in a sudden increase in the dT/dP melting slope, which is usually preceded by a portion of the melting line exhibiting a negative, vanishing, or very small, positive slope. Although the specific mechanism

Table 1. Summary of anomalous properties for five soft core potentials we have studied in three dimensions. These anomalies include rich polymorphism of crystal phases (PCP), re-entrant melting, (RM) anomalous increase of compressibility upon cooling (AIK) resulting in κ_T maximum (KTM), anomalous increase of C_P upon cooling (AIC) sometimes resulting in C_P maximum (CPM), anomalous thermal expansion (ATE) upon cooling, anomalous increase of diffusivity upon pressurizing (AID), liquid–liquid phase transition (LLPT) and polyamorphism of glassy states (PAGS). The latter may be observed in the form of a sharp (S), first-order-like transition, or gradual (G) hysteretic changes of the structure upon pressurizing.

| Potential | PCP | RM | AIK | AIC | ATE | AID | LLPT | PAGS |
|-----------|-----|-----|-----|-----|-----|-----|------|------|
| Shoulder | Yes | Yes | KTM | Yes | No | No | No | G |
| SSSW | Yes | Yes | KTM | CPM | No | No | Yes | S |
| Ramp | Yes | Yes | KTM | Yes | Yes | Yes | No | G |
| Jagla | Yes | Yes | KTM | CPM | Yes | Yes | Yes | S |
| Exp-6 | Yes | Yes | KTM | Yes | Yes | Yes | No | G |

at work may differ substantially, such behaviors can be interpreted, in the effective-potential approach, to be effects of the weakening of repulsive forces associated with the crossover from a larger to a smaller repulsive length scale. We may expect this to be a general phenomenon that induces any substance to settle into a more compact and rigid arrangement if the pressure is high enough. A regularly increasing and concave melting line typical of, e.g., hard sphere and inverse-power potentials, although assumed for a long time to be standard behavior, is actually unrealistic at extreme pressures. Anomalous melting can be expected to be the norm among the elements. However, the pressures and temperatures at which structural softening occurs can vary considerably from one substance to another, as suggested by how the location of exp-6 anomalies are extremely dependent on the steepness of the repulsion. In principle, larger and heavier atoms should be more susceptible, at least within the same chemical family, to pressure-induced modifications in condensed phases. This is consistent, for example, with the known properties of alkali metals [88, 120, 122–126] and with the behavior of rare gases, in which the flattening observed in the melting line at high pressures is more marked and occurs at a lower pressure in the heavier gases [121, 127].

4. Summary

We show that soft core potentials can reproduce many anomalous properties of substances at low temperatures. These results are summarized in table 1. While all these phenomena are not necessarily associated with one another, they all come from the same origin, namely the ability of the soft core models when pressurized to collapse and restructure.

As we have seen from various studies, most of the soft core potentials exhibit crystal polymorphism but not all of them exhibit liquid anomalies and LLPT. The presence of an attractive part in the potential seems to be a necessary condition for the existence of an LLPT and sharp polyamorphism in the glassy states. In cases without a LLPT, pressurizing of glassy states results in a gradual transition from one state to another. The potentials with a narrow region of strong

repulsive forces, such as those with a square shoulder and SSSW, do not exhibit density and diffusivity anomalies, but still show a compressibility maxima line that seems to be the most ubiquitous of the thermodynamic anomalies present in the models we studied. To observe density and diffusivity anomalies, a wider, ramp-like region of repulsive forces is needed. The heat capacity increases upon cooling in all of these models, but only in models with a clear LPPT does it develop a maximum in the equilibrium liquid state associated with the Widom line as well as the non-ergodic maximum at the glass transition. From the examples studied here, it is clear that re-entrant melting is not always associated with a density anomaly. Our preliminary studies show that density anomalies may exist even in the absence of re-entrant melting. We also clearly see that a density anomaly and an LLPT can exist independently of each another. In all cases studied, the LLCP lies outside the density anomaly region, resulting in a positive slope of the LLPT line. As the slope of the LLPT line approaches zero, the critical point disappears below the line of homogeneous nucleation [42] and becomes undetectable in computer simulations. We also demonstrate that the density minimum and the compressibility maximum are not necessarily related to the Widom line emanating from an LLCP. The density minimum and heat capacity maximum occur near the glass transition and may not indicate the Widom line. To conclude, an observation of one anomalous feature in an experiment leaves open a wide variety of possible scenarios regarding the observation of other anomalies in the behavior of the substance under investigation.

Acknowledgments

We thank F Mallamace, S-H Chen, S Sastry and F W Starr for helpful discussions, and NSF grant no. CHE 0404673 for support. CAA acknowledges support from NSF-DMR grant no. 0454672. LX acknowledges support from World Premier International Research Center Initiative (WPI Initiative), MEXT, Japan. We also thank the Boston University Computation Center for allocation of CPU time. LX thanks the allocation of computations time on SGI Altix 3700B×2 at the Advanced Fluid Information Research Center, Institute of Fluid Science, Tohoku University. SVB thanks the Office of the Academic Affairs of Yeshiva University for funding the Yeshiva University high-performance computer cluster and acknowledges the partial support of this research through the Dr Bernard W Gamson Computational Science Center at Yeshiva College.

References

- [1] Hemmer P C and Stell G 1970 *Phys. Rev. Lett.* **24** 1284
- [2] Stell G and Hemmer P C 1972 *J. Chem. Phys.* **56** 4274
- [3] Young D A and Alder B J 1977 *Phys. Rev. Lett.* **38** 1213
- [4] Debenedetti P G, Raghavan V S and Borick S S 1991 *J. Phys. Chem.* **95** 4540
- [5] Head-Gordon T and Stillinger F H 1993 *J. Chem. Phys.* **98** 3313
- [6] Johnson M E, Head-Gordon T and Louis A A 2007 *J. Chem. Phys.* **126** 114509
- [7] Cho C H, Singh S and Robinson G W 1996 *Phys. Rev. Lett.* **76** 1651
- [8] Cho C H, Singh S and Robinson G W 1996 *Faraday Disc. Chem. Soc.* **103** 19
- [9] Stillinger F H and Stillinger D K 1997 *Physica A* **244** 358
- [10] Sadr-Lahijany M R, Scala A, Buldyrev S V and Stanley H E 1998 *Phys. Rev. Lett.* **81** 4895
- [11] Sadr-Lahijany M R, Scala A, Buldyrev S V and Stanley H E 1999 *Phys. Rev. E* **60** 6714
- [12] Sadr-Lahijany M R, Scala A, Giovambattista N, Buldyrev S V and Stanley H E 2001 *Phys. Rev. E* **63** 041202
- [13] Jagla E A 1998 *Phys. Rev. E* **58** 1478
- [14] Jagla E A 1999 *J. Phys.: Condens. Matter* **11** 10251
- [15] Jagla E A 1999 *J. Chem. Phys.* **111** 8980
- [16] Jagla E A 2001 *Phys. Rev. E* **63** 061501
- [17] Jagla E A 2001 *Phys. Rev. E* **63** 061509
- [18] Jagla E A 2001 *Phys. Rev. Lett.* **86** 3206
- [19] Jagla E A 2004 *Braz. J. Phys.* **34** 17
- [20] Franzese G, Malescio G, Skibinsky A, Buldyrev S V and Stanley H E 2001 *Nature* **409** 692
- [21] Franzese G, Malescio G, Skibinsky A, Buldyrev S V and Stanley H E 2002 *Phys. Rev. E* **66** 051206
- [22] Malescio G, Franzese G, Pellicane G, Skibinsky A, Buldyrev S V and Stanley H E 2002 *J. Phys.: Condens. Matter* **14** 2193
- [23] Buldyrev S, Franzese G, Giovambattista G, Malescio G, Sadr-Lahijany M R, Scala A, Skibinsky A and Stanley H E 2002 *Physica A* **304** 23
- [24] Brazhkin V, Buldyrev S V, Ryzhov V and Stanley H E (ed) 2002 *New Kinds of Phase Transitions: Transformations in Disordered Substances* (Dordrecht: Kluwer)
- [25] Buldyrev S V and Stanley H E 2003 *Physica A* **330** 124
- [26] Skibinsky A, Buldyrev S V, Franzese G, Malescio G and Stanley H E 2004 *Phys. Rev. E* **69** 061206
- [27] Malescio G, Franzese G, Skibinsky A, Buldyrev S V and Stanley H E 2005 *Phys. Rev. E* **71** 061504
- [28] Kumar P, Buldyrev S V, Sciortino F, Zaccarelli E and Stanley H E 2005 *Phys. Rev. E* **72** 021501
- [29] Yan Z, Buldyrev S V, Giovambattista N and Stanley H E 2005 *Phys. Rev. Lett.* **95** 130604
- [30] Xu L, Kumar P, Buldyrev S V, Chen S-H, Poole P H, Sciortino F and Stanley H E 2005 *Proc. Natl Acad. Sci. USA* **102** 16558
- [31] Yan Z, Buldyrev S V, Giovambattista N, Debenedetti P G and Stanley H E 2006 *Phys. Rev. E* **73** 051204
- [32] Netz P A, Buldyrev S V, Barbosa M C and Stanley H E 2006 *Phys. Rev. E* **73** 061504
- [33] Xu L, Buldyrev S V, Angell C A and Stanley H E 2006 *Phys. Rev. E* **74** 031108
- [34] Buldyrev S V, Kumar P, Debenedetti P G, Rossky P G and Stanley H E 2007 *Proc. Natl Acad. Sci. USA* **104** 20177
- [35] Yan Z, Buldyrev S V, Kumar P, Giovambattista N, Debenedetti P G and Stanley H E 2007 *Phys. Rev. E* **76** 051201
- [36] Yan Z, Buldyrev S V, Kumar P, Giovambattista N and Stanley H E 2008 *Phys. Rev. E* **77** 042201
- [37] Xu L, Buldyrev S V, Giovambattista N, Angell C A and Stanley H E 2009 *J. Chem. Phys.* **130** 054505
- [38] de Oliveira A B, Franzese G, Netz P A and Barbosa M C 2008 *J. Chem. Phys.* **128** 064901
- [39] de Oliveira A B, Netz P A and Barbosa M C 2009 *Europhys. Lett.* **85** 36001
- [40] Camp P J 2003 *Phys. Rev. E* **68** 061506
- [41] Camp P J 2005 *Phys. Rev. E* **71** 031507
- [42] Gibson H M and Wilding N B 2006 *Phys. Rev. E* **73** 061507
- [43] Wilding N B and Magee J E 2002 *Phys. Rev. E* **66** 031509
- [44] Rzyzsko W, Pizio O, Patrykiewicz A and Sokolowska S 2008 *J. Chem. Phys.* **129** 124502
- [45] Cervantes L A, Benavides A L and del Rio F 2007 *J. Chem. Phys.* **126** 084507

- [46] Lomba E, Almarza N G, Martin C and McBride C 2007 *J. Chem. Phys.* **126** 244510
- [47] Fomin Y D, Gribova N V, Ryzhov V N, Stishov S M and Frenkel D 2008 *J. Chem. Phys.* **129** 064512
- [48] Bosio L, Chen S-H and Teixeira J 1983 *Phys. Rev. A* **27** 1468
- [49] Soper A K and Ricci M A 2000 *Phys. Rev. Lett.* **84** 2881
- [50] Botti A, Bruni F, Isopo A, Ricci M A and Soper A K 2002 *J. Chem. Phys.* **117** 6196
- [51] Strassle T, Saitta A M, Le Godec Y, Hamel G, Klotz S, Loveday J S and Nelmes R J 2006 *Phys. Rev. Lett.* **96** 067801
- [52] Canpolat M, Starr F W, Sadr-Lahijany M R, Scala A, Mishima O, Havlin S and Stanley H E 1998 *Chem. Phys. Lett.* **294** 9
- [53] Schwegler E, Galli G and Gygi F 2000 *Phys. Rev. Lett.* **84** 2429
- [54] Saitta A M and Datchi F 2003 *Phys. Rev. E* **67** 020201R
- [55] Sciortino F, Geiger A and Stanley H E 1990 *Phys. Rev. Lett.* **65** 3452
- [56] Sciortino F, Geiger A and Stanley H E 1991 *Nature* **354** 218
- [57] Adam G and Gibbs J H 1956 *J. Chem. Phys.* **43** 139
- [58] Errington J R and Debenedetti P G 2001 *Nature* **409** 318
- [59] Esposito R, Saija F, Saitta A M and Giaquinta P V 2009 *Phys. Rev. E* **73** 040502
- [60] Errington J R, Truskett T M and Mittal J 2006 *J. Chem. Phys.* **125** 244502
- [61] Yan Z, Buldyrev S V and Stanley H E 2008 *Phys. Rev. E* **78** 051201
- [62] Mishima O, Calvert L D and Whalley E 1985 *Nature* **314** 76
- [63] Poole P H, Sciortino F, Essman U and Stanley H E 1992 *Nature* **360** 324
- [64] Angell C A 1983 *Annu. Rev. Phys. Chem.* **34** 593
- [65] Aasland S and McMillan P F 1994 *Nature* **369** 633
- [66] Wilding M C, Wilson M and McMillan P F 2006 *Chem. Soc. Rev.* **35** 964
- [67] Hohl D and Jones R O 1994 *Phys. Rev. B* **50** 17047
- [68] Katayama Y 2002 *J. Non-Cryst. Solids* **312** 8
- [69] Katayama Y, Mizutani T, Utsumi W, Shimomura O, Yamakata M and Funakoshi K 2000 *Nature* **403** 170
- [70] Sheng H W, Liu H Z, Cheng Y Q, Wen J, Lee P L, Luo W K, Shastri S D and Ma E 2007 *Nat. Mater.* **6** 192
- [71] Sastry S and Angell C A 2003 *Nat. Mater.* **2** 739
- [72] Morishita T 2004 *Phys. Rev. Lett.* **93** 055503
- [73] McMillan P F 2005 *Nat. Mater.* **4** 680
- [74] Rapaport E 1968 *J. Chem. Phys.* **48** 1433
- [75] Bhat H, Molinero V, Solomon V, Soignard E, Sastry S, Yarger J L and Angell C A 2007 *Nature* **448** 787
- [76] Molinero V and Moore E B 2009 *J. Phys. Chem. B* **113** 4008
- [77] Meade C, Calvert R J and Mao H K 1992 *Phys. Rev. Lett.* **69** 1387
- [78] Poole P H, Hemati M and Angell C A 1997 *Phys. Rev. Lett.* **79** 2281
- [79] Saika-Voivod I, Poole P H and Sciortino F 2001 *Nature* **412** 514
- [80] Hemmati M, Moynihan C T and Angell C A 2001 *J. Chem. Phys.* **115** 6663
- [81] Angilella G N, Leys F E, March N H and Pucci R 2003 *Phys. Chem. Liq.* **41** 211
- [82] Brazhkin V V, Voloshin R N, Popova S V and Umnov A G 1992 *J. Phys.: Condens. Matter* **4** 1419
- [83] Tse J S and Klug D D 1999 *Phys. Rev. B* **59** 34
- [84] Katayama Y 2001 *J. Synchrotron. Radiat.* **8** 182
- [85] Kurita R and Tanaka H 2005 *J. Phys.: Condens. Matter* **17** L293
- [86] Sciortino F 2005 *J. Phys.: Condens. Matter* **17** V7
- [87] Scandolo S 2002 *Proc. Natl Acad. Sci. USA* **100** 3051
- [88] Bonev S A, Schwegler E, Ogitsu T and Galli G 2004 *Nature* **431** 669
- [89] Pfaffenzeller O and Hohl D 1997 *J. Phys.: Condens. Matter* **9** 11023
- [90] Boates B and Bonev S A 2009 *Phys. Rev. Lett.* **102** 015701
- [91] Poole P H, Saika-Voivod I and Sciortino F 2005 *J. Phys.: Condens. Matter* **17** L431
- [92] Paschek D 2005 *Phys. Rev. Lett.* **94** 217802
- [93] Kauzmann W 1948 *Chem. Rev.* **43** 219
- [94] Tveryanovich L S, Ushakov V M and Tverjanovich A 1996 *J. Non-Cryst. Solids* **197** 235
- [95] Tsuchiya Y 1999 *J. Non-Cryst. Solids* **250** 473
- [96] Liu D Z, Zhang Y, Chen C C, Mou C Y, Poole P H and Chen S H 2007 *Proc. Natl Acad. Sci. USA* **104** 9570
- [97] Mallamace F, Branca C, Broccio M, Corsaro C, Mou C Y and Chen S H 2007 *Proc. Natl Acad. Sci. USA* **104** 18387
- [98] Sen S, Andrus R L, Baker D E and Murtagh M T 2004 *Phys. Rev. Lett.* **93** 125902
- [99] Sastry S, Debenedetti P G, Sciortino F and Stanley H E 1996 *Phys. Rev. E* **53** 6144
- [100] Liu L, Chen S H, Faraone A, Yen C W and Mou C Y 2005 *Phys. Rev. Lett.* **95** 117802
- [101] Buldyrev S V 2008 *Aspects of Physical Biology (Springer Lecture Notes in Physics)* ed G Franzese and M Rubi (Berlin: Springer) p 97
- [102] Giovambattista N, Angell C A, Sciortino F and Stanley H E 2004 *Phys. Rev. Lett.* **93** 047801
- [103] Kanno H and Angell C A 1980 *J. Chem. Phys.* **73** 1940
- [104] Moynihan C T, Macedo P B, Montrose C J, Gupta P K, Debolt M A, Dill J F, Dom B E, Drake P W, Eastale A J, Elterman P B, Moeller R P, Sasabe H and Wilder J A 1976 *Ann. New York Acad. Sci.* **279** 15
- [105] Elsaesser M S, Kohl I, Mayer E and Loerting T 2007 *J. Phys. Chem. B* **111** 8038
- [106] Debenedetti P G 2003 *J. Phys.: Condens. Matter* **15** R1669
- [107] Johari G P, Hallbrucker A and Mayer E 1987 *Nature* **330** 552
- [108] Winkel K, Elsaesser M S, Mayer E and Loerting T 2008 *J. Chem. Phys.* **128** 044510
- [109] Loerting T and Giovambattista N 2006 *J. Phys.: Condens. Matter* **18** R919
- [110] Young D A 1991 *Phase Diagrams of the Elements* (Berkeley, CA: University of California Press)
- [111] Likos C N 2001 *Phys. Rep.* **348** 267
- [112] Mausbach P and May H O 2006 *Fluid Phase Equilib.* **249** 17
- [113] Buckingham R A 1938 *Proc. R. Soc. A* **168** 264
- [114] Fried L E, Howard W M and Souers P C 2002 *12th Int. Detonation Symp. (Aug. San Diego)*
- [115] Malescio G, Saija F and Prestipino S 2008 *J. Chem. Phys.* **129** 241101
- [116] Frenkel D and Smit B 2001 *Understanding Molecular Simulation* (New York: Academic)
- [117] Prestipino S, Saija F and Malescio G 2009 *Soft Matter* **5** 2795
- [118] Angell C A 2004 *Annu. Rev. Phys. Chem.* **55** 559
- [119] Debenedetti P G 1998 *Metastable Liquids: Concepts and Principles* (Princeton, NJ: Princeton University Press)
- [120] Jayaraman A, Newton R C and McDonough J M 1967 *Phys. Rev.* **159** 527
- [121] Ross M, Boehler R and Soderlind P 2005 *Phys. Rev. Lett.* **95** 257801
- [122] Bundy F P 1959 *Phys. Rev.* **115** 274
- [123] Gregoryanz E, Degtyareva O, Somayazulu M, Hemley R J and Mao H 2005 *Phys. Rev. Lett.* **94** 85502
- [124] Raty J Y, Schwegler E and Bonev S A 2007 *Nature* **449** 448
- [125] Gregoryanz E, Goncharov A F, Matsuishi K, Mao H and Hemley R J 2003 *Phys. Rev. Lett.* **90** 175701
- [126] Zha C S and Boehler R 1985 *Phys. Rev. B* **31** 3199
- [127] Boehler R, Ross M, Soderlind P and Boerker B 2001 *Phys. Rev. Lett.* **86** 5731
- [128] Meijer E J and Frenkel D 1991 *J. Chem. Phys.* **94** 1169
- [129] Saija F, Prestipino S and Giaquinta P V 2006 *J. Chem. Phys.* **124** 244504
- [130] Saija F, Malescio G and Prestipino S 2009 *Phys. Chem. Liq.* submitted (doi:10.1080/00319100903131542)